WORDT
NIET UITGELEEND

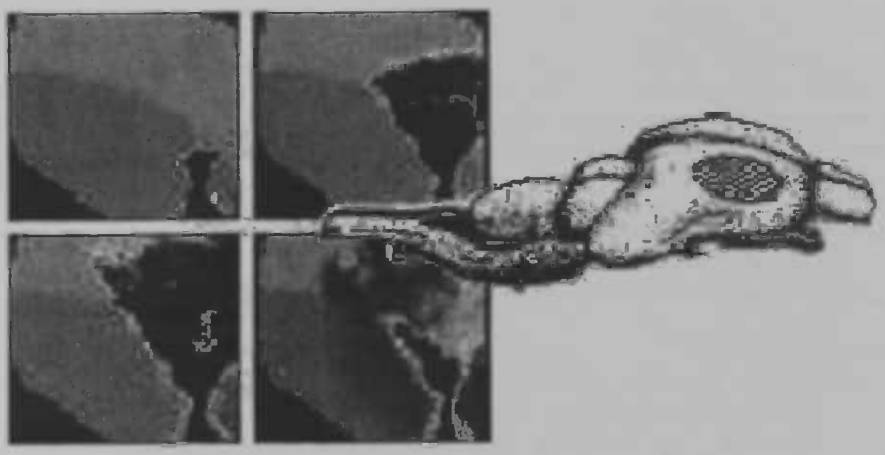

Hebbian Learning in the Freshwater Turtle Visual Cortex

Zac Freudenburg

supervisors:

Bijoy K. Ghosh, Washington University St. Louis

Michael Wilkinson, Rijksuniversiteit Groningen, afdeling informatica

November 16, 2004

Contents

Abstract

The Hebbian synaptic weight learning rule is the most basic and wide spread learning rule used in neuromodeling. However, to date there has been little work done in applying this simple learning mechanism to significantly large-scale cortex models. The visual cortex of a freshwater turtle, when stimulated by a pattern of light, produces waves of activity that have been both recorded experimentally and simulated using a large scale model cortex. It has been shown using the model cortex that the cortex waves encode spatial information of visual input and can be used for detection. This paper explores the effects of Hebbian learning on the wave activity patterns of the freshwater cortex model.

Rijksuniversiteit Groningen
Bibliotheek Wiskunde & Informatica
Postbus 800
9700 AV Groningen
Tel. 050 - 363 40 01

1 Introduction

The human spirit has always been one of curiosity and discovery. Throughout his history man has strived for a higher understanding of the world he lives in, his origin and purpose in his world, and even worlds beyond his. To this extent man has been uniquely successful among his co creatures on earth. Yet relatively little is understood about the organ that drives this curiosity. The sheer complexity of the human brain and human dependency on it limitations makes it one of the most difficult explorations man has embarked on. In the last century a greatly increased knowledge base of the anatomical structures that characterize the brain has lead to a better understanding of the global mechanisms that govern the functions of everyday. However, the details of these mechanisms and how they lead to higher learning and understanding are still quite fussy. This paper addresses small area of research into the details of these mechanisms.

The Center for BioCybernetics and Intelligent Systems (CBCIS) lab headed by Professor Bijoy Gosh at Washington University in St. Louis has developed a computer model of the visual cortex of a fresh water turtle. The visual cortex is the area of the brain that responds to visual information and the model was created based on turtle cortex anatomical and imaging research. It is believed that the visual cortex response encodes spatial information of visual stimuli. The CBCIS has been able to detect the location of input in the simulated visual field based on the response of the primary excitation cells in their model. The focus of this paper is to take this model and gain a further understanding of its behavior through studying the effects of introducing simple Hebbian synaptic learning. It is not conclusively known whether synaptic learning is a true feature of the fresh water turtle visual cortex, but the following learning discussion illuminates interesting features of the cortex model. When these features are seen in the general scope of neural networks that balance excitation and inhibition to produce global wave responses to input, they give insight into the benefits to be gained from Hebbian learning. These insights can be useful in the growing search for engineering applications of such networks.

The discussion on Hebbian learning in the cortex model is begun with an introduction of the basic aspects of neural research and the historical and current context of the Hebbian learning mechanism within this context. Then the details of how the turtle cortex is modeled and the features of the model are handled in the second section of the paper. The third section presents the results of introducing Hebbian learning into the model in terms of it effects on the model features. Finally the significance of these effects are disused in the concluding section. The introduction begins with a more detailed outline of the paper structure in the following section.

1.1 Organization

Neural research is a very broad topic and the following introduction sections build only a sparse contextual framework of the field. Section 1.2.1 lays a foundation of general biological neural network aspects. This is followed by a discussion of neural network modeling issues and motivation in section 1.2.2. Section 1.3 reinforces the Hebbian learning and the cortex model in the general context of neural biological fundamentals. Next, Hebbian learning is discussed in more detail in placed in historical and current context in sections 1.4 and 1.5 respectively.

Once the basic context and motivation of neural research and Hebbian learning have been established the methods and materials used to create the model are discussed in the second section of the paper. The most important and relevant turtle cortex features to the cortex model are discussed in section 2.1. The basic compartmental neural modeling technique and how is was used to model turtle visual cortex is covered in section 2.2. Next, the response of the cortex model and how it relates to the real cortex response are talked about in section 2.3, followed by a discussion of the features the basic model response to stimulus input in section 2.4. The methods used to further analyze and compare the model response to different stimulus are presented in to section 2.5. This concludes the material and methods of the established cortex model. Section 2 concludes by introducing the method used to include Hebbian learning into the model in section 2.6.

Based on the analysis of the model response spatial classification of the input stimulus can be made. For reasons discussed in the introduction and materials and methods sections, introducing Hebbian learning into the model can be expected to change the model response. The ways in which the model response is changed are handled by looking

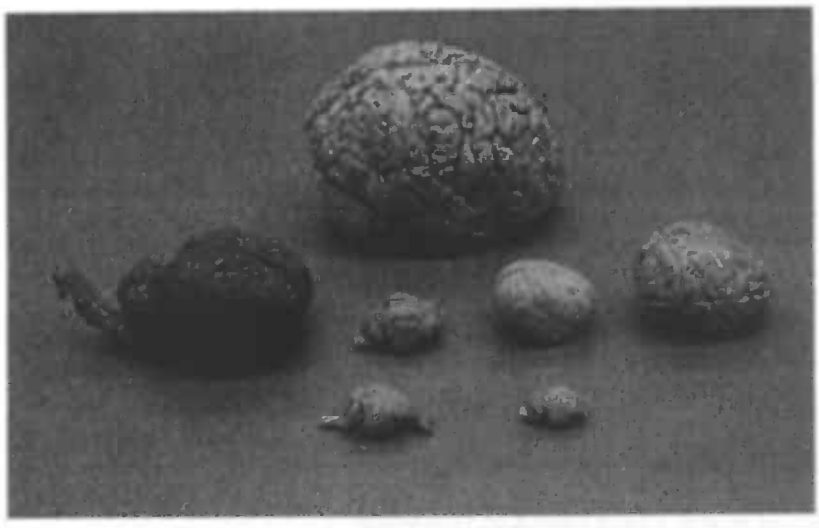

Figure 1: The human (top), camel (middle left), cat (middle second from left), chimpanzee (middle second from right), baboon (middle right), rabbit (bottom left), and squirrel (bottom right) brain. [45]

at changes in main response features in the third section of the paper. These changes are covered individually in sections 3.1 through 3.5.

Finally, the paper concludes by reviewing the model response features changes due to the implementation of Hebbian learning in section 4.1. This is followed by a discussion of directions for the continuation of the research dealt with in this paper in section 4.2.

1.2 Context and Motivation

In comparison with the computational abilities of today's computers, biological brains are able to process more information much faster and perform much more complicated tasks. What biological 'brains' have in common that make them such powerful computers are neuron cells working together in very large network structures. In fact the most powerful computer know to man, the human brain, has on average 100 billion neurons [36] that work together to form the control unit that coordinates sensory input and performs the reflexive, reactive, and cognitive tasks of everyday life.

1.2.1 Biological Brains

While all brains are made up of collections of neuron cells, more advanced vertebrate brains share three basic properties. They are split down the middle into two hemispheres, they are connected to the rest of the nervous system at the base by the spinal cord, and they delegate different control tasks to different brain areas. The two hemispheres and other general brain shape features can be seen in figure 1. The outermost layer of the hemispheres is called the cortex.

As mentioned above different areas of the brain are dedicated to different tasks. Figure 2 shows the global control units of the human brain. The simplest involuntary, reflexive, and coordinative tasks are taken care of by the small pons area and cerebral areas closest to the entrance of the brain stem. The sight, sound, and touch incoming sensory information is responded to by the occipital, temporal, and parietal lobes, while the frontal lobe controls the ability to speak. The true thinking is done in the cerebrum. Here information form the sensory input lobes is coordinated and turned into voluntary physical and verbal responses, emotions, thoughts, ideas, and memories. These areas of higher cognitive tasks are part of the outer cortex layer.

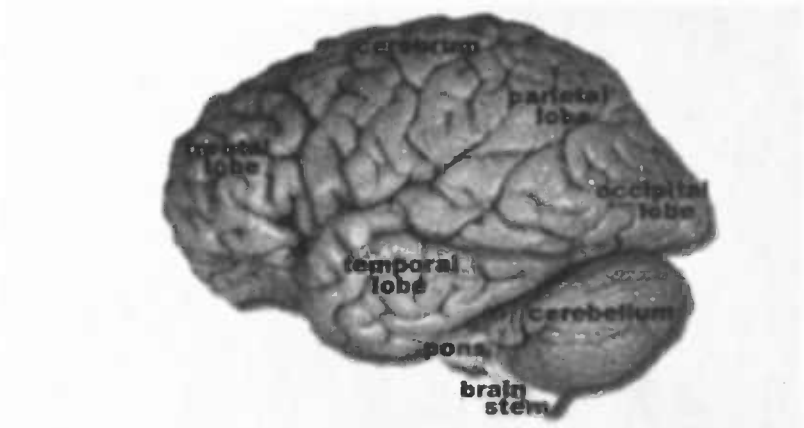

Figure 2: Dorsal view of a turtle brain. OB, olfactory bulb; CTX, cortex; OT, opic tectum; CB, cerebellum. 2

Species whose behaviors are considered to be mainly reflexive or instinctive have relatively larger cerebellum areas. This can be seen in the camel, cat, rabbit, and squirrel brains of figure 1. Species that display more complex social behavioral patterns can be seen to have relatively larger cortex areas. As can be seen in figure 1, more recently evolved "higher" mammals have folds in the cortical tissue [42]. This folding increases the amount of cognitive tissue by increasing surface area of the cortex.

Neural tissue structure is considered to be much more indicative of cognitive ability then brain mass. For example, the cow's brain is slightly larger (425 to 500 grams) then the chimpanzee's brain (approximately 420 grams) [36], yet monkeys are considered one of the most intelligent species on earth while the cow is general considered to have little higher cognitive ability. This is most likely due to the fact that the structure of the monkey brain closely resembles that of a human brain. These two species also demonstrate that the brain-to-body mass ratio as an indication of cognitive ability. A cows brain is only 0.1% of its body mass, while the brain of a human is 2.1% of body mass. However, a mouse has a brain-to-body mass ratio of 3.2% [38]. While mice are often used as the subjects of behavioral studies because of their relatively high cognitive capacity few argue that mice are intellectually superior to humans. Thus, this ratio is still not as important as the actual brain tissue structure. Mice brains contain a relatively large cortical area. However their cortical hemispheres are smooth and lack the cortical folds that are that are a dominant characteristic of the human cortex.

A turtles brain is also smooth approximately the same mass as a mouse's (0.3 gram)) [36]. As indicated by the fact that a turtle that has lost its sight or cannot smell due to pneumonia will not eat, turtles depend greatly sight and smell, and perhaps falls a bit short in its cognitive problem solving abilities [37]. Accordingly, the turtle brain has highly developed sight and smell centers. As can be seen from indicated oval-shaped region in figure 3, the visual cortex is a predominant part of the turtle cortex, making it accessible for laboratory research.

1.2.2 Artificial Brains

The idea of modeling a biological neural network with computer software to try and learn from biology has been around for about 50 years [46]. Each neuron in a neural network can be seen as a single computational unit that receives input signals from its input connected neighboring neurons and passes a functional translation of these signals to its output connected neurons. In this way an originating stimulus signal coming from a sensory organ or another part of the brain is rapidly responded to by a large number of neurons. By changing the properties of the synaptic connections between the neurons the flow of the signals through the network can be controlled. It is the combined response of the network that is the true output or computational result of the network. The corruption or removal of a few connections or neurons will not drastically change overall network response. The parallel

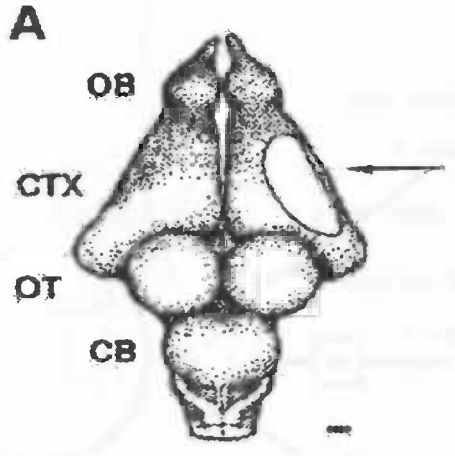

Figure 3: Dorsal view of a turtle brain. OB, olfactory bulb; CTX, cortex; OT, opic tectum; CB, cerebellum.

computing and robust nature of neural networks make them very useful tools for many computational jobs.

For instance robust pattern recognition can be done with a simple feed-forward network that passes input from an input layer of neurons, through a single hidden layer, to an output layer of neurons. Such a network structure is depicted in figure 4. The input pattern is presented as activation values on the input layer of neurons. The hidden layer neurons are identical computational nodes that simply pass on the Sigmoid function [8]value of the weighted sums of their received input layer connection signals to their output layer connections. Each output layer neuron in turn computes a weighted sum of its received signals to determine its value. Each output layer neuron is associated to a specific pattern category. The input is then recognized as the being of the category of the output neuron with the highest resulting value. Which output neuron this is is determined by the weights of the network connections and the input values. The network serves as a weighted map from input patterns to activation of a dominant output neuron. If the weights are set properly then inputs that possess one set of basic features will be mapped to one output neuron will inputs that share a different set of features will be mapped to another. The changing of one single weight may change to output neuron activation level slightly, but chances are the same one will still be dominated. This basic network is very simple, yet it illustrates the basic computational method of neural networks.

There is a lot that can be learned about information processing possibilities of neural networks by gaining a better understanding of the basic properties of biological neural networks. However, most computer scientists are primarily concerned with application possibilities of artificial neural networks (ANN). While ANNs are inspired by the properties of biological neural systems, they do not strive to model the true workings of biological neural networks. This is because simple ANNs, such as the one described above, can achieve many of the tasks desired in computer science today and biological neural networks can be very involved systems to model.

To illustrate this complexity consider the fact that there are at least 10^{11} neurons, each with, on average, 1000 synaptic connections. This results in the order of 10^{14} total connections in the human brain [14], meaning that there are more synapse in the human brain then than there are stars in the galaxy. If the weight value of each synaptic connection were stored in one byte of memory then a 100,000 GB memory would be necessary to just store the weights. Considering that 250 GB is top of the line as far as disk space in a PC goes these days, this highlights the infeasibility of starting with complete neural network models.

By reducing the number of neurons included to a small fraction of the actual number and dividing the brain

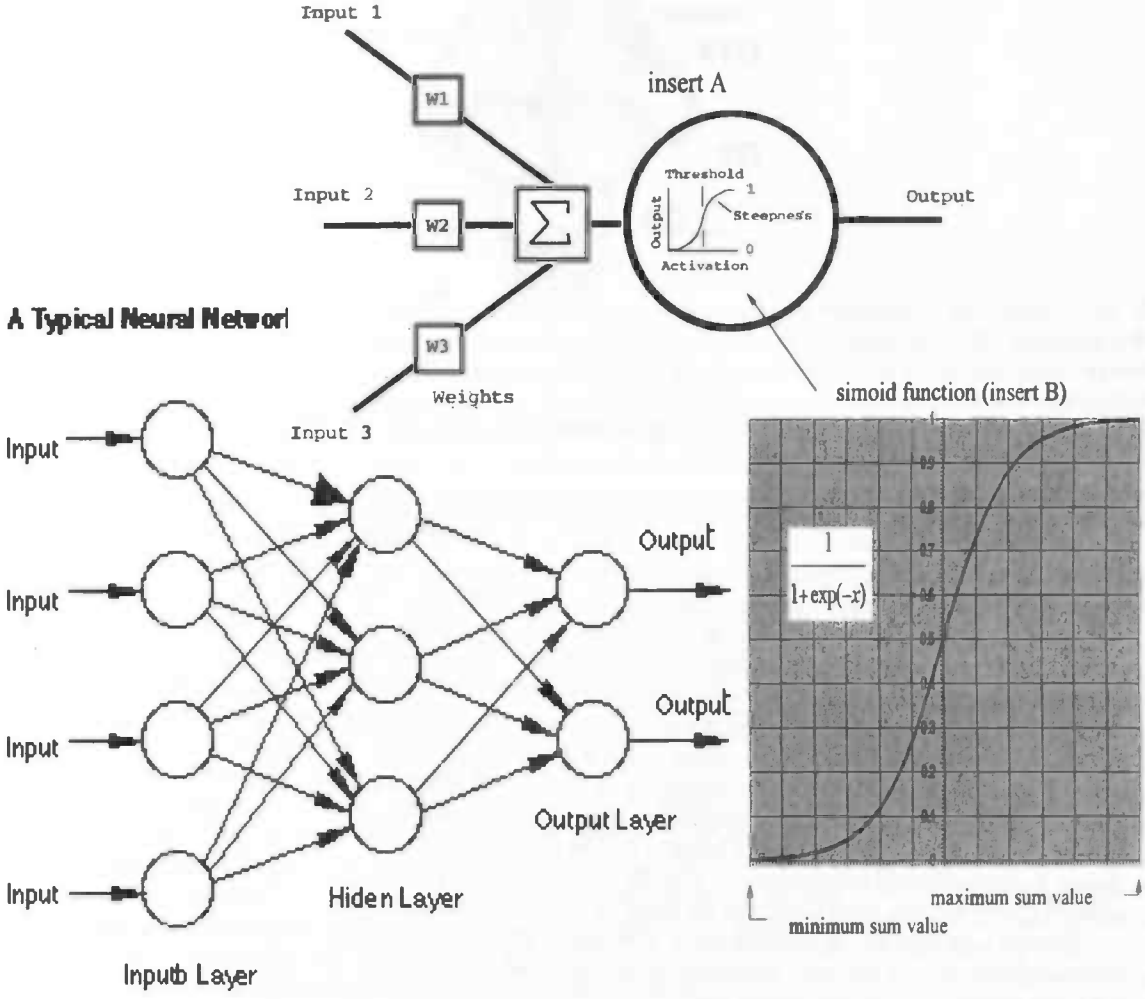

Figure 4: Simple single hidden layer feed forward neural network. (insert A) Single neuron output value calculation [39]. (insert B) The sigmoid function [35].

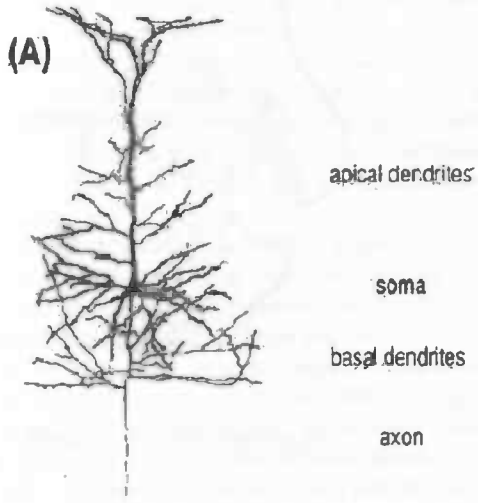

Figure 5: The four basic sections of a pyramidal neuron

and even single neurons into modeled subsections, models can be created that give insights into basic biological neural network properties. Understanding the true biomechanics of brains is key to accurately making these complexity reductions. Thus, most neural modeling is done by neural scientists. However, taking a computer scientist's perspective of the network behavior and practical functionality of the models can aid in the understanding of them.

Silicon neuromorph systems that closely resemble real neural networks have already been developed [16]. The relatively slow speed of biological neural units compared to silicon gates further demonstrates the potential of man-made neural networks. Because software changes are practically free compared to hardware modifications, researchers turn to software-based neural models to develop the understanding needed begin to reach the full potential of this technology.

It is clear that the advancement of neural science and computer science are becoming more and more interdependent. This is perhaps most evident in the field of neural modeling.

1.3 Basic Biology behind Neural Networks

As mentioned above, the basic building blocks of a neural network are its neurons. Biological neurons are special kinds of cells that communicate with each other using electrical signals. A neuron is made up of three main parts, as depicted in figure 5. Signals are received from a collection of many hair-like receptors called dendrites. These dendrites propagate the signals they receive through neural membrane tissue to the cell nucleus, called the Soma. The Soma produces a series of electrical pulses that vary in amplitude and frequency in response to the signals coming in through the dendrites. The response signal then travels along the neural membrane of the cell's tail, the axon. Nodes at the end of the axon, called synapses, pass the response signal to the dendrites of other cells. In this way signals propagate through the network of synaptically connected neurons.

The specific properties of the neurons and connections can vary widely. In many biological networks two opposing types of neurons exists. Excitatory neurons work to stimulate other neurons and promote activity among the neurons, while inhibitory neurons work to dampen and even kill activity among other neurons when they are stimulated.

As with ANNs, information is stored in the properties of the connections between the neurons. As mentioned

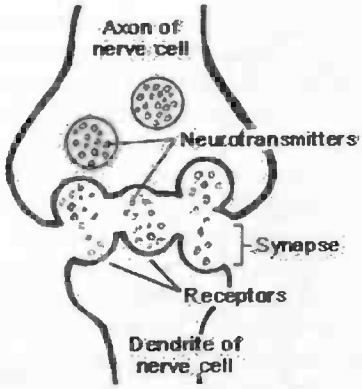

Figure 6: Chemical synapses

above, these connections come in the form of synapses between the axons and dendrites of the neuron cells. The part of the channel connected to the signal-sending axons is considered the pre-synaptic half of the synapses, while the part connected to the signal-receiving dendrite is considered the post-synaptic end of the synapses. Synaptic connections can be either electrical or chemical [14]. Electrical synapses connect the pre-synaptic and post-synaptic neurons with a connecting membrane, which allows signals to pass virtually undelayed across the channel. Electrical signals are not directly transmitted across a connecting membrane in chemical synapses. Instead, pre-synaptic ion channels are activated that release vesicles containing chemical neurotransmitters that cross a narrow extra-cellular space to post-synaptic receptors on the dendrites of 'connected' cells [14]. Figure 6 diagrams the structure of a chemical synapse.

Chemical synapses are slower, with a transmission delay of 1 to 5 ms, yet much more diverse in the transmission properties and adaptive then electrical synapses [14]. Chemical synapses are able to pass inhibiting signals or amplified signals. Also, the strength of these connections can be varied with the number of synaptic channels present. In this way the number of synaptic channels acts as the weighting factor for the connection. Because of their diverse properties chemical synapses are the dominant connection type found in cognitive neural structures, while electrical synapses are general limited to sensory and reflexive neural organs.

As highlighted above, the networks built from the neurons are often very large and complex with many layers and connections. While the number and types of neurons an organism has are generally fixed genetically, the connections between them remain plastic or changeable throughout the life cycle. Prenatal development establishes the neural structure of the brain, yet the pattern of neural connections seen at birth only roughly approximates the wiring of the brain at death [15]. In fact, 'neuroplasticity' is defined as the 'lifelong ability of the brain to reorganize neural pathways based on new experiences' [9]. Thus, an organism's cognitive capacity is in a sense genetically fixed, while the way it which it uses this capacity to perceive and react to its world is learned through experience.

By the time a human infant is two or three years old, the approximately 2,500 synapses per neuron they had at birth has grown to approximately 15,000 synapses per neuron [7]. However, this amount is reduced by half, through a process called 'synaptic pruning', by the time adulthood is reached. Connections that have been activated most frequently are strengthened and preserved and infrequently active connections are pruned. Thus, experience determines which connections will survive the early stages of life. This process may seem wasteful but one study shows that memory performance is maximized if synapses are first overgrown and then pruned [2]. The wiring of the brain determines in large part perceptual and social ability.

Evidence of this was shown by Marius von Senden's work with children born with cataracts that severely interfere with the optics of the eye, but do not physically interfere with the nervous system [15]. While cataracts can be removed in infants resulting in no permanent vision impairment, Von Senden found that children who did not get their cataracts removed until a later age (10 to 20) were permanently impaired in there ability to perceive form. Research done comparing emotionally isolated babies to babies given normal or higher levels of attention also

suggests that not only perceptive abilities but also behavioral traits are permanently affected by the early synaptic development [15].

Synaptic plasticity does not only occur during development to maturity. The synapses that survive development continue to change their characteristics until death, facilitating the brain's ability to retain new information. While some evidence supports the concept that short-term memory depends upon electrical and chemical events in the brain as opposed to structural changes of synapses after a period of time, information must be moved into a more permanent type of long-term memory. Long-term memory is the result of anatomical or biochemical changes that occur in the brain [29].

However, patients with head injuries have shown that synaptic adaptation in later stages of life can also drastically alter perceptual ability. In studies involving rats in which one area of the brain was damaged, brain cells surrounding the damaged area underwent changes in their function and shape that allowed them to take on the functions of the damaged cells [9]. Although this phenomenon has not been widely studied in humans, some studies indicate that similar changes occur in human brains following injury. Patients who have suffered damage to the area of the brain responsible for perceiving color become color blind if the damage was extensive enough to prevent this area of the brain from reacting to the color sensory signals. Yet in some patients their ability to perceive color returns after a year or so. It has been shown that in these cases the brain had adapted to reroute color stimuli to a new area of the brain. The most biologically feasible and experimentally evident mechanism for learned adaptation of synapses is the Hebbian mechanism, which strengthens synaptic connections that regularly take part in stimulating other neurons and weakens connections that often pass a signal that is not responded to by the destination neurons. Thus, in the case above, the brain damage to the color perception area of the brain keeps this area of the brain from responding to color information in visual stimulus resulting in the weakening of the connections to this areas of the brain. This can be seen as forcing the signals to be route elsewhere and once other area of the brain begins to react to these signals these connections are strengthened. Hebbian synaptic learning is discussed in more detail in section 1.4.

Only the tip of the iceberg of complexity of the brain has been presented here. A very comprehensive discussion of the neural biology is given in [12].

1.4 A Brief History of Hebbian Learning

In 1949 Canadian neuropsychologist Donald O. Hebb kick-started research into neural networks when he published his book, "The Organization of Behavior" [8].

At this time pioneering work by physiologists such as Ramn y Cajl at the turn of the 20th century was being built on with new research by neurobiologists such as Hodgkin and Huxley to produce an exciting new understanding of brain anatomy. All biological 'brains' have two things in common. First, they mainly consist of neural cells that when significantly stimulated by electrical signals produce a pattern of electrical pulses whose frequency is dependent on the stimulus strength [12]. Secondly, there exist chemical synaptic connections between these cells that are able to rapidly transmit the electrical signals throughout the brain [12].

These two main physiological features gave rise the connectionist notion that the electrical state of neurons and the properties of their synaptic connections represent ideas and cognitive thoughts in the brain. This idea was formalized to form the basis of modern connectionism. The first principle of connectionism states that any given mental state can be described as an n-dimensional vector of numeric activation values over neural units in a network [33]. The second asserts that memory is created by modifying the strength (weight) or the architecture of the connections between neural units [33].

In 1948 McCulloch and Pitts gave mathematical validity to connectionism by showing that a network constructed with a sufficient number of connected identical neural units with properly set connection properties could in principle compute any computable function [8]. The McCulloch-Pitts model simplified neural units as computational units that passed on a sum of their received input signal strengths if the sum is above a given threshold and connection transition properties as single weight factors [8].

However, it was Hebb who first presented an explicit statement of a physiological learning rule for synaptic modification. Without such a rule the modern tenet of neural science that 'all behavior is a reflection of brain function' [12] would have to exclude learned behavior.

Hebb desired a theory of behavior that reflected the physiology of the brain as closely as possible. Based on the existence of continuous cerebral activity within the brain and Cajl's postulate of learning Hebb argued for the existence of a mechanism that allows neurons that are repeatedly simultaneously active to increase their ability to communicate with each other. Cajl's postulate of learning states that the effectiveness of a variable synapses between two neurons is increased by the repeated activation of one neuron by the other across that synapses [8]. Hebb's postulate assert that, when an axon of cell A is near enough to excite a cell B and repeatedly or persistently takes part in firing it, some growth process or metabolic change takes place in one or both cells such that A's efficiency, as one of the cells firing B, is increased. [8]. Hebb also went a step further to include the decay of the efficiency of cell A's ability to fire cell B when it's axon is near enough to excite cell B yet fail to do so.

Hebb's postulate was later formalized into the Hebbian Learning Rule. Returning to the language of connectionism, the Hebbian Learning Rule states that the weight of a connection between two neurons is increased if both the source (pre-synaptic) neuron and the target (post-synaptic) neuron are actively simultaneously and it is decreased if the two neurons are active separately [18]. Logically the Anti-Hebbian Rule states that the weight is decreased through simultaneous and increased through opposing activity. Both of these rules include the added assertion that when both neurons are inactive no learning takes place.

In 1958 Stephen Grossberg derived the 'gated steepest descent' rule, which is also considered the Hebbian/anti-Hebbian Rule because it recognizes the importance of a balance between Hebbian and anti-Hebbian mechanisms in a stable learning law. Grossberg's Rule also includes a real-time learning aspect because the adapted weight of the synapse is represented in a differential equation. However, at this time too little was know about how biological learning developed to support such a learning rule.

1.5 Current Research Activity involving Hebbian Learning

The basic Hebbian learning rule presented above can be quite limited. The rule is unsupervised and can lead to an exponential increase in the synaptic weights, which produces unstable network states. For this reason many variations of the Hebbian rule have been developed and are in use today. One of these rules is the Hopfield Law that introduces a learning rate into the Hebbian rule, which mediates the magnitude with which a synaptic weight changes in response to pre or post-synaptic activity [41].

In 1960 Widrow and Hoff took a new look at the Hebbian rule from a engineering perspective and developed the Delta Rule, is perhaps the most popular Hebbian variation rule in use today [40]. The Delta Rule is based on the idea of continuously modifying the strengths of the input connections to reduce the difference (the delta) between the desired output values and the actual output of a neuron [41]. Rules such as the Delta rule are considered supervised because they take into account a desired result state. When this desired state is calculated for the output layer of a feed forward ANN, such as the one discussed in section 1.2.2 on page 6, and passed back to as the desired output used to calculated the desired state of preceding layers, it is called 'error back-propagation' learning. These types of supervised rules lend themselves better to use in neural network applications and most work involving artificial neural networks has moved far beyond the basic Hebbian rule.

Although any learning algorithm that adjusts synaptic weights to better represent the relationship between neurons (and thus even supervised back-propagation rules) can be considered Hebbian in nature, the basic Hebbian rule stated above remains the most biologically feasible. For this reason, simple variations of the basic Hebbian rule are still quite common in biological neural modeling research. In fact recent research, such as the work done in Kandel's lab which shows evidence for the involvement of Hebbian learning mechanisms at synapses in the marine invertebrate Aplysia Californica [34] and the work done at the Center for Neural Basis of Cognition that shows Hebbian strengthening in the synaptic connections of a honeybee's brain [6], has only served to strengthen the case for the simple Hebbian learning process being a major contributor in biological neural networks. This combined with resent advances in imaging techniques such as positron emission tomography (PET) [13] and the use of multi-electrode arrays and voltage sensitive dyes that facilitate the creation of more accurate neural network models have brought simple Hebbian learning back to the forefront of biological neural network research.

Contributing to the resurgence of Hebbian learning usage in neural network research is the ever-clearer importance of anti-Hebbian learning. Research, such as that done by Morgan and Andrade showing the crucial role

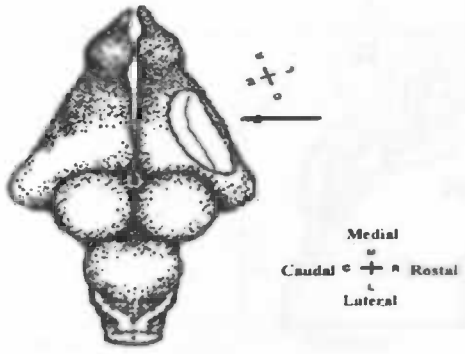

Figure 7: Turtle brain and visual cortex spatial coordinates.

of anti-Hebbian learning in the development of cortical neuron receptive fields [19], has served to establish anti-Hebbian learning as a central peace of the learning puzzle.

2 Materials and Methods

The neural network model discussed in this paper follows in Hebb's footsteps in the fact that it also strives to closely simulate the behavior of a biological neural network. The features of the turtle cortex that make it an interesting subject for modeling and the methods used to do so are discussed in the following sections.

2.1 The Freshwater Turtle Visual Cortex

The biophysical knowledge used by the CBCIS to create an accurate model of the cortex was contributed largely by the work of Ulinski at the University of Chicago. In depth discussions of the cerebral cortex of reptiles [30] and the visual pathways in turtles [31] are given in Ulinski's work. The network behavior of the turtle cortex has been recorded and studied using surgically removed visual pathways with normal afferent connections preserved among the retina, lateral geniculate complex, and visual cortex by Senseman et al at The University of Texas at San Antonio [28]. The knowledge gained from this work provides a reference of comparison for the CBCIS models. A brief description of the biophysical and behavioral aspects of the cortex most important to the discussions of this paper is presented below.

2.1.1 Biology of the Freshwater Turtle Visual Cortex

Figure 7 demonstrate the turtle brain, and accordingly visual cortex, coordinate terms that are commonly used. The front and back of the brain (top and bottom of the diagram in figure 7) are considered the rostral and caudal poles respectively. The top and bottom of the brain are respectively considered the medial and lateral poles. These coordinates will be used throughout this paper. As seen in figure 7, the visual cortex, indicated by the oval outline, makes up a large percentage of the turtle cortex area. The cortex is split into two regions. These regions are called the lateral and medial regions corresponding to their orientation in the brain coordinates.

Figure 8 shows a coronal section through the cerebral cortex at the level indicated by the arrow in figure 7.

The type of excitatory neurons found in the turtle cortex is called pyramidal because of their three-dendrite branch shape. An example of such a cell is shown in figure 5. Each region is characterized by it's own type of

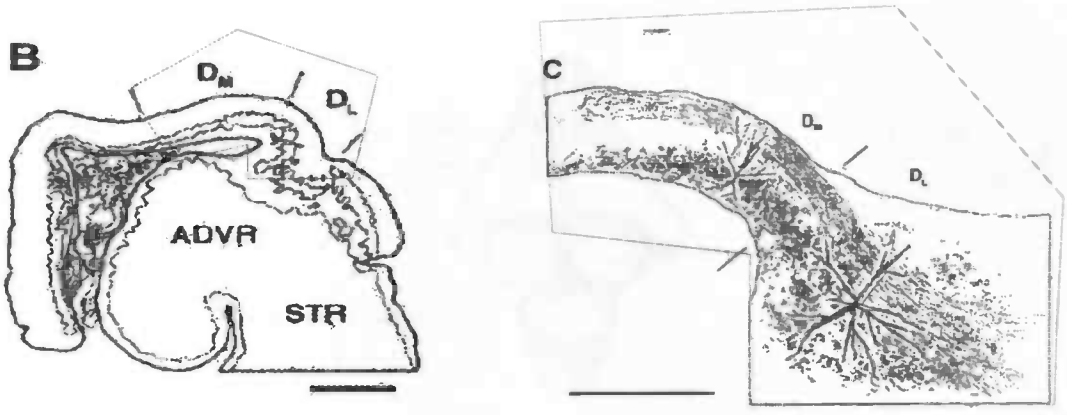

Figure 8: (B) Coronal section through the cerebral cortex. (C) Detailed view of visual cortex area outlined in red showing the position of a lateral (blue) and medial (green) pyramidal cell (the original drawing by Dr. J. B. Colombe has been edited for this paper). In both diagrams, the dorsal medial and dorsal lateral halves of the cortex are indicated by DM and DL respectively.

pyramidal cell situated as shown in the detailed view in figure 8C. Connecting to cells in both of these regions are three types of inhibitory cells; the faster-reacting subpial cells, horizontal cells, and slower-reacting stellate cells. There are three basic layers of the cortex. The intermediate layer contains mostly pyramidal cells with dendrites that extend into the outer layer and inner layer of the cortex. The outer and inner layers contain mostly inhibitory neurons [32]. LGN cells have axons that connect to the dendrites of the intermediate layer pyramidal neurons and outer layer neurons. All connections are made via chemical synapses.

The turtle cortex is stimulated by a group of dorsal lateral geniculate neurons (LGN) that bridge the gap between it and the turtle's retinal cells. There are far fewer LGN neurons than retinal neurons in the turtle brain. This fact suggests that the visual information is greatly reduced in complexity though a kind of data-compression filter before it is encoded in the cortex.

2.1.2 Behavior of the Freshwater Turtle Visual Cortex

Many visual cortexes demonstrate a spatial mapping of retinal activity in one area of the retinal field to a specific group of cells in the cortex. This is not the case in the visual cortex of a freshwater turtle. When paralyzed turtles are alerted by 0.5 spots of light for 100 to 500 ms, single units throughout the visual cortex respond independent of the stimulus location in the binocular space [17]. It has been shown by using both multieletrode arrays [23] and voltage sensitive dyes [26] [27] that the turtle cortex generates a planar 'wave' of activity that moves from the rostral pole across the entire cortex to the caudal pole. In addition, Prechtl et al have reported observing very complex propagating waves including circular or spiraling waves [23]. It has also been shown that distinctly different stimuli produce waves with reproducible distinguishing characteristics [28], despite the intrinsic noise introduced into the cortex response due to the stochastic properties of chemical synapses and voltage-gated channels [4].

The propagation properties of these waves have been further studied using the cortex models developed by the CBCIS [4] [5] [21]. The model evidence supports the notion that visual information such as position and velocity of objects in the visual field are encoded in these cortex waves. There is no direct evidence as of yet that this information is used by the turtle in visual tasks. It has been shown that turtles have a minimal visual response time of 150ms, which is seen to be the minimal time necessary for the onset of cortical waves using both the in vivo multieletrode array [23] and voltage sensitive dye [26] [27] techniques mentioned above. However, at this time the waves have only begun to move across the cortex. It is believed that the waves serve to prolong the time the turtle

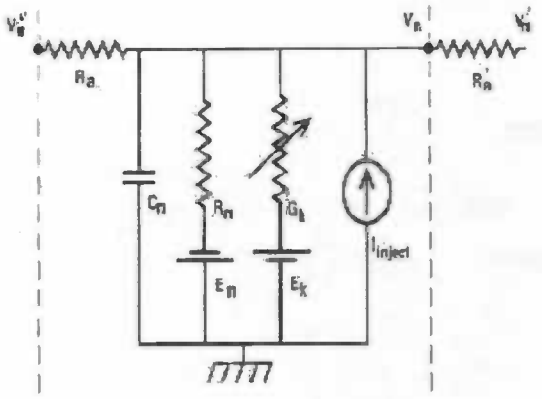

Figure 9: Example of a compartment circuit representing a the electrical properties of a membrane section. [1]

has to fully respond to the visual information and possibly make the predictions about future locations of objects necessary to catch fish under water.

2.2 Neural Networks Modeling

True neural networks are complicated and computationally expensive to model due to the drastic number and complex behavior of the components involved. Thus, simplifications need to be made to make software implementations possible. As mentioned above, in the case of ANNs the simplest model needed to get the desired computational job done is sought.

Yet, in striving to understand the working of biological networks, models that reflect true neural anatomy and the knowledge gained from ever improving imaging techniques, are the goal. Thus, simplifications that preserve these characteristics are sought. In this section the techniques used to create the freshwater turtle cortex model and the extent to which it accurately reflects the real turtle cortex feature are discussed.

2.2.1 Compartmental Modeling of Biological Neural Networks

As its name implies, the compartmental modeling technique models a neuron by breaking it up into compartments. Each compartment models a section of the neuron cell and its signal transmission properties. This can be done because neural membranes have been shown to behave as simple electrical circuits with some capacitance, resistance, and voltage and current sources, such as the one in figure 9 [1]. This is also the basic principle behind the silicon neuromorph network models mentioned in section 1.2.2 on page 6.

In this way, differences in voltage between the connected compartments produces an electrical current that propagates through the cell. The somata are often depicted as spherical compartments and take the electrical form of a circuit with capacitors that control the spiking voltage discharge pattern of the modeled soma. The dendrites are in turn usually depicted as cylindrical compartments. The axons are modeled as simple resistor delay lines. The inhibitory cells exert inhibition simply by inducing a negative current in respect to the basic current direction of an excitatory cell.

Thus each compartment is actually a series of equations describing an electrical circuit that behaves electrically equivalent to the modeled compartment. The accuracy of the neuron model depends on the accuracy of the compartment equations in describing their corresponding neuron section. Generally as the sections to be modeled get larger their electrical properties become less uniform, which makes describing them with a single circuit less accurate. Therefore, the neuron should be broken down into its electrically uniform membrane sections. However, the com-

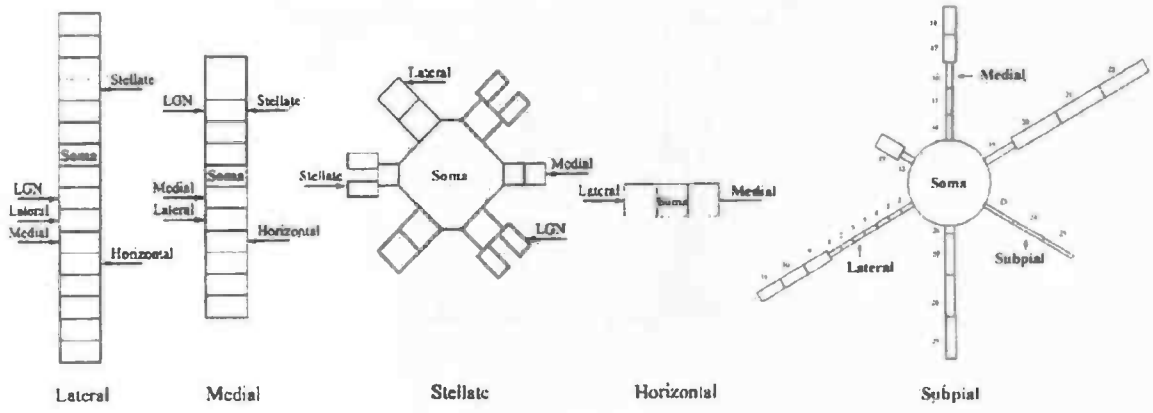

Figure 10: Compartmental layout of model lateral, medial, stellate, horizontal and subpial cells

putational resources often limit the number of compartments that can feasibly be modeled. The challenge is to find a membrane division that maximizes inter-compartment uniformity while minimizing the number of compartments.

2.2.2 Modeling the Turtle Cortex

The cortex model was created using the GENESIS software developed at Caltech. GENESIS uses the common compartmental model technique to model individual neurons and allows these neurons to be connected in a network with modeled synaptic channel connections.

The numbers, spatial distributions, and connectivity of the neurons are based on anatomical research done mainly by Mulligan and Ulinski. The model contains 368 lateral and 311 medial pyramidal cells, 45 stellate cells, 44 subpial cells, and 20 horizontal cells. Compartmental models of the five cell types used in the model are pictured below in figure 10. A detailed description of compartmental models of the medial, lateral, stellate, and subpial cells is given in [22]. The compartmental model of the subpial cells is presented in [32].

The numbers of cells of each type preserve the ratios found in the real cortex and represent about 1 percent of the actual numbers. Maps of the spatial distribution of neurons in each of the three layers were constructed from coronal sections. The maps were divided into 8×56 array rectangular areas. The neuron positions within each region are randomly assigned consistent with the ratios of neuron types found in the biological cross section of the cortex. The three layers of the cortex are projected onto a signal plane in the model as shown in figure 11.

Noise is introduced into the cortex in the form of random small stimulus injected into the soma of each cell. This produces a certain level of cortex activity even when no input signal is present.

In order to get propagation of a wave the network must be stimulated beyond the noise levels. This is done by a group of 201 LGN neurons. Biophysical data are not available for neurons in the dorsal lateral geniculate complex of turtles, so LGN neurons were modeled as single compartments with a spike generating mechanism.

The work by Nenadic et al provides more detail into the spatial neuron distribution, simulated noise, and LGN neuron components of the cortex model [22].

2.2.3 Connecting the Turtle Cortex

The network is not fully connected. Only connections between certain types of neurons and within a limited distance of each other are connected. Figure 12 below shows which cell types are connected [32]. The compartmental

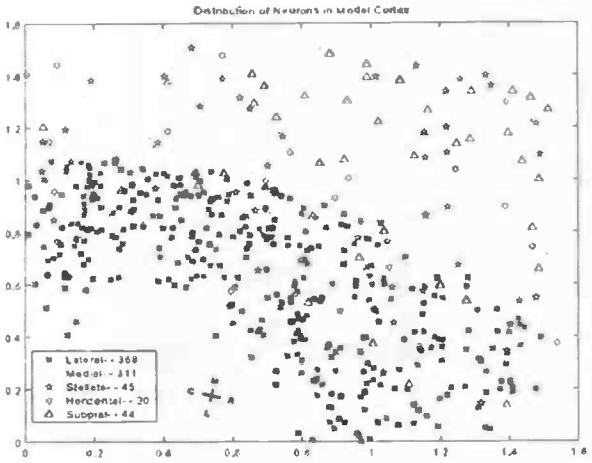

Figure 11: Spatial layout of the cortex cells

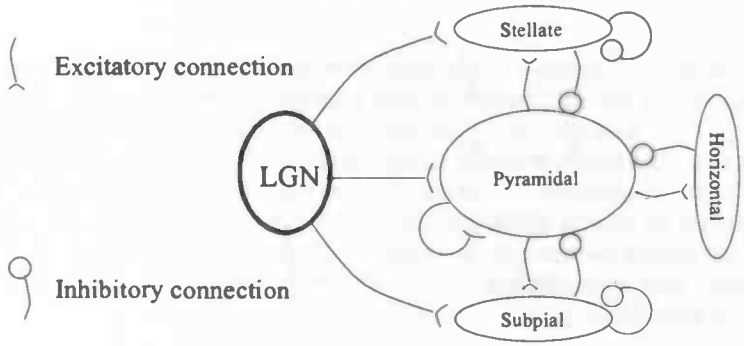

Figure 12: Connection diagram

model diagrams in figure 10 also indicate the compartments to which the connections are made. The biologically determined spheres of connection determine the radius value for a spherical area of connectivity for each neuron type.

Geniculate axons were modeled as delay lines that extend across the cortex. The LGN neurons are linearly arranged along the lateral edge of the cortex with axons extending into the cortex as shown in figure 13. The axons are implemented as simple delay lines with velocities and varicosities constrained by biophysical data. The varicosity of an axon determines the positions of nodes along the axons. The nodes then transmit the axon signal to the pyramidal, stellate, and subpial cells within a given radius. In the model a direct synaptic connection is made between an LGN cell and the cortex cells that are influenced by the nodes along its axon based on the distance between the LGN and the given node plus the distance between the node and the given cortex cell. Further details of the geniculate cell connections to the model are also given in [22].

While physical chemical synaptic channels may contain many synapses, only one synapse, per channel, per connection between two neurons is used in the model. Synaptic channels are modeled as synaptic currents of the form

$$I = gmax * g(t) * V(t) \tag{1}$$

where, $V(t)$ is the instantaneous membrane potential, $g(t)$ is the time course of the conductance, and $gmax$ is the

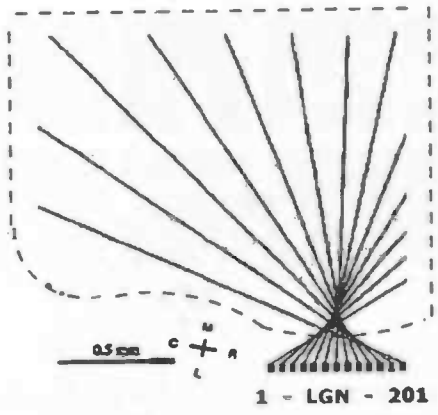

Figure 13: LGN Axon spatial distribution pattern

maximum conductance value reached. Each spike message to a channel establishes a synaptic connection and increments synapse objects that each have there own weight and delay values [1]. Since the model only uses one synapse per channel, there is simply one weight and delay value for each connection between two cells.

The wave behavior of the freshwater turtle visual cortex is made possible by a delicate balance between inhibitory and excitatory neurons. The number of synaptic channels per each type of connection weights the connections in such a way to maintain the balance between excitation and inhibition needed to allow wave propagation. However, since our model only models one synapse per channel, the balance is kept simply in the weights associated with the channel connections. Thus, after trial and error weight values that produce a wave of activity that closely models the biological waves were found [22].

2.3 The Model Cortex Response

As with any neural network, either artificial, modeled, or real, neurons stimulated by the LGN input neurons in the cortex model respond and pass their activity on to other neurons in the network. FSigure 14 shows the response of 16 pyramidal neurons, without noise stimulus, to a simulated diffuse light flash input from the LGN neurons. The 8 neurons of figure 14 A represent a lateral-to-medial transect of the cortex, and the neurons in figure 14 B represent a rostral-to-caudal transect. Due to the delay line feature and spatial distribution of the LGN axons, the rostral-lateral pole of the cortex is stimulated first. This is directly reflected in the transects of figure 14. However, it is difficult to visualize a wave pattern simply from the voltage potential recordings of the model.

The cortex response waves can be visualized in 'movies' depicting the voltage potentials of the pyramidal cells at 1ms intervals color-coded over a two dimensional grid. The voltages potentials were used because they most closely represent the activity images captured by Precht and Senseman [27]. The interpolation method used to complete the voltage picture between the neurons and the resemblance of the movies to Precht and Senseman's movies are discussed in [21]. Eight time frames of two activity movies can be seen in figure 15. In the movies higher activity is represented by warmer colors whereas lower activity is reflected by cooler colors. The figure shows that simulated waves also move from the rostral pole, located at the right of the simulated pyramidal space, to the caudal pole, located on the left side.

While the model a has been shown to have wave responses that bounce off the caudomedial pole under certain input conditions [32], the model has not been shown to display the complex spiral waves seen in Prechtl's in vivo preparations [23]. It is not know whether this is to an insufficiency in the model or just simple because the right

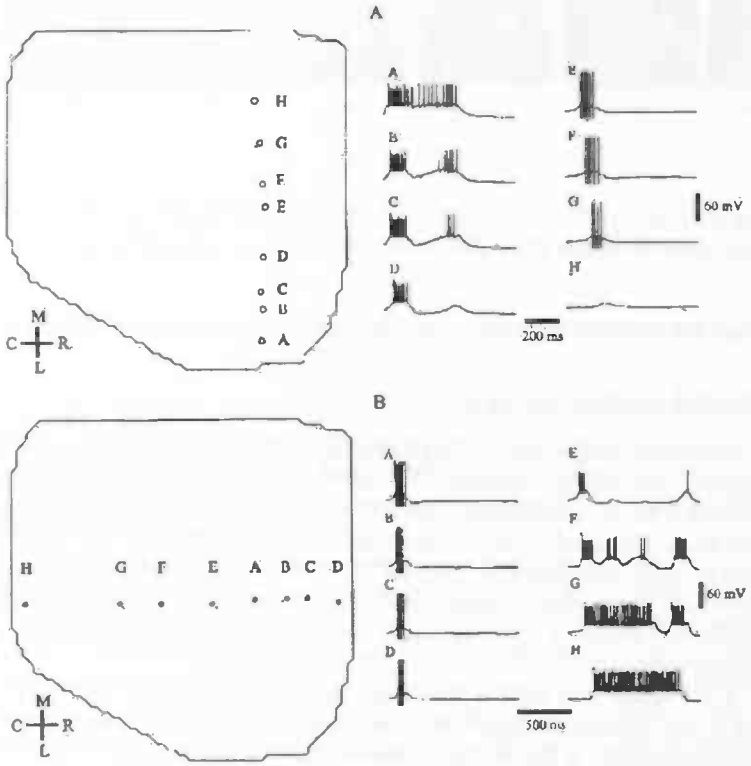

Figure 14: The firing patterns of lateral (A-D) and medial (E-H) cells along a vertical (A) and horizontal (B) transect of the cortex space in response to an LGN simulated light flash input. [21]

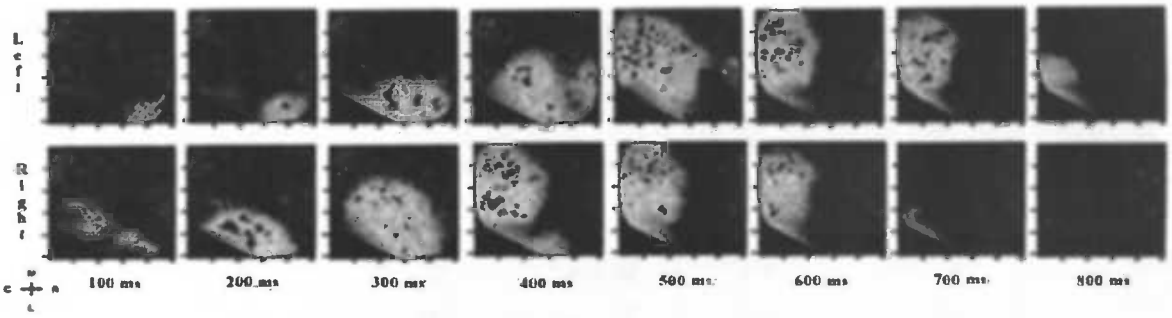

Figure 15: (Top): 8 frames of a left movie. The frames are from left to right at simulations times 100, 200, 300, 400, 500, 600, 700, and 800 ms.(bottom): 8 frames of a right movie at the same corresponding simulation times

input conditions to cause these waves have not yet been used. The waves presented below are simple plane waves.

2.4 Features of the Model Cortex Waves

Typically the LGN cells are stimulated using a single voltage pulse of a sufficient width in time and height in current strength to produces a pyramidal wave activity response. The activity waves depicted in figure 15 were the results of a pulse of 150 ms in width and 9 pA in height applied to the first or left most 20 cells (top) and last or right most 20 cells (bottom) in the LGN array. These cells will be considered respectively the 'left' and 'right' input locations throughout the paper. As can be seen from figure 13, the first 20 LGN cells stimulate the rostral-lateral corner of the cortex while the last 20 LGN cells stimulate a larger area stretching from the rostral-lateral corner diagonally in the caudal medial direction. The first frames of figure 15 clearly show that the origin of the pyramidal activity wave directly reflects the LGN stimulus location.

Once stimulated, cells in the origin area send signals back and forth reinforcing each other's activity. The firing of one pyramidal cell is not enough to trigger the firing of a connected pyramidal cell alone. It takes a number of pyramid cells working together to fire another pyramidal cell. However, sufficient input stimulus from a LGN neuron can fire a pyramidal cell. Also, pyramidal cells experience an activity dip below their resting voltage potentials after they have fired. Left on its own, a pyramidal cell will not quickly recover from this dip. For these reasons, it is important that the input signal remains long enough to build up enough activity to allow pyramidal cells to sufficiently stimulate each other to the point of sustaining the origin area activity and collectively firing pyramidal cells beyond the origin area. At this stage the activity becomes self-propagating and inhibition is required to constrain it. This happens at approximately 100 to 200 ms in the simulations time, which corresponds well to the 150ms wave onset time seen in the real cortex.

The difference in wave origin due to LGN location gives rise to a visual distinction in the activity propagation patterns seen in the activity movies. Perhaps the most obvious difference is the speed with which the waves propagate and die. It can be clearly seen from figure 15 that the right wave reaches the caudal pole and dies faster than the left wave.

Further analysis of the frames in figure 15 gives insight into the mechanisms behind the wave-like activity behavior of the cortex and the distinction between left and right waves.

As discussed, activity remains localized in the origin area until enough activity is built up to sufficiently stimulate cells outside the origin area. Then a rapid expansion of activity takes place, as seen in the third frame of the left wave in figure 15. Continuing the story through the point of view of the left wave, frame 4 shows that the explosion of activity causes the inhibition cells to react and kill the activity in the origin area. The wave effect is caused by the fact that the activity is able to stay one step ahead of the inhibition and resurge, as seen in frame 5 until it runs into the caudal boundary. The activity can then no longer move further and the following rush of inhibition finally overcomes the activity and the wave dies, as seen in the final frame.

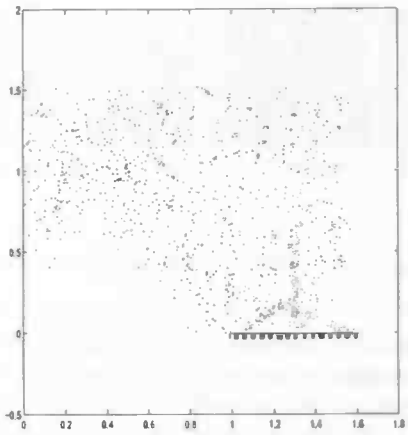

Figure 16: Diagram summeriesing the input situation

The story of the right wave reads the same as the left only faster. The quicker pace can be directly attributed to the difference in wave origins. As mentioned above, the right origin is larger and stretches closer to the causal pole. Hence, the larger initial activity seed leads more rapidly to the expansion phase and has less room to run before it hits the causal pole. The increased activity also triggers a larger inhibition response that more quickly overcomes the activity once it is catches up to it.

The frames of figure 15 also introduce another important feature of the cortex model. It can be seen from these frames that the areas of the cortex that were stimulated during the propagation of the wave are left in a state of much lower pyramidal activity after the wave has moved on than before the wave. Thus, just as with most waves in nature, the wave leaves an area of depression in its wake. The pyramidal cell resting potential recovery period mentioned above causes this activity depression. While the recovery period is modeled after the properties of pyramidal cells, it is not clear whether this collective activity depression is also a property of the real cortex because the activity imaging techniques mention above are much poorer in resolving low activity then they are in showing high activity.

It should be noted that the difference in left and right activity origins also causes a bias between left and right LGN input in the model. This bias can be seen in the strength of the input pulse needed to produce a propagating wave. The minimum strength of a pulse of width 150 ms applied to the 20 left input neurons is approximately 6 pA, while that for the right 20 LGN neurons is approximately 8 pA.

While it is not clear whether this bias also exists in the real cortex, it can be explained by the model by two main characteristics. First, there exists a fundamental difference in the varicosity distribution of the LGN axons. As can be seen from figure 15, the larger right initial activity area causes the varicosity points along the LGN axons for the right input regions to cover a less dense area stretching farther away from the LGN cell origin then those along the left input regions. When there is sufficient stimulation to support pyramidal cell to pyramidal cell activity reinforcement, the larger origin area of the right stimulus causes more initial activity. However, the fact that the LGN axons' varicosity points are less dense means that the pyramidal cells that are stimulated by them will be further apart from each other. Thus each pyramidal cell will have fewer other stimulated cells close enough to reinforce it. Also, because the varicosity points are on average farther away from the base of the LGN axon, the synaptic connections made with the pyramidal cells will have on average longer delay lines. This also contributes to a weakening of the signal. The LGN axon varicosity differences lead to a fundamental bias of approximately 0.1 pA favoring input from the left even when all inhibitory cells have been removed from the cortex model. When the inhibition cells are reintroduced to the model, the bias is increased to the values (6 pA verse 8 pA) mentioned above.

The fact that the bias is considerably decreased when the inhibitory cells are removed from the model identifies them as a primary suspect in causing the bias. The fact the spatial distribution of inhibitory cells in the cortex is not uniform suggests means by which the bias can exist. Since stellate and subpial cells are directly connected to

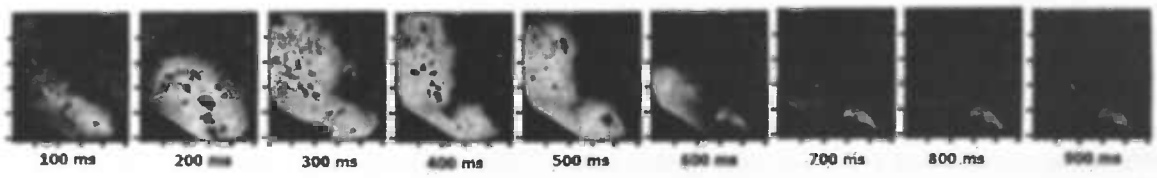

Figure 17: Frames at 100 ms intervals from 100-900 ms of the cortex response to 900 ms of continuous right input

LGN axons they will also be stimulated by the same input that stimulates the pyramidal cells. Figure 16 shows the location of the varicosity points stimulated by left and right input relative to the location of the subpial cells in the cortex. The scells are focused on because they respond very quickly (< 10 ms) to the stimulus while the stellate cells are much slower to respond and the horizontal cells can only respond to the pyramidal activity itself. It can be seen from figure 15 that there is a disparity in the number of subpial cells that inhibit the input based on LGN location. This disparity is greatest at the edges. As can be seen from the figure, input from the far right will stimulate four subpial cells and input from the far left stimulates no subpial cells. Thus, it seems likely that the even greater bias seen when the inhibitory cells are present in the model is due largely to the subpial cell distribution. Further attention will be paid to this bias later in this paper, but for now it should be noticed that the simulations are run with a strong enough input pulse to cause a wave reaction from both the left and right side.

Figure 17 shows the cortex response to a continuous input pulse of strength of 8 pA applied to the right input position. The simulation was allowed to continue under the presence of the input stimulus until 1500ms. Despite the continued presence of input stimulus, the cortex model only responds with one initial wave that is similar to the right response wave in figure 15. This emphasizes the fact that it is not the stop in input that causes the wave of activity to move from the rostral to caudal pole and die. It is the inhibitory response of the horizontal, stellate, and subpial cell that push the activity across the cortex and eventually kill it altogether.

This simulation also demonstrates that the activity depression following wave propagation prevents the cortex from being able to further respond to stimulus. It has also been shown that when the stimulus is removed once the wave begins to propagate and not reapplied for a substantially long time (2000ms) that the model is still unresponsive to further input. Thus, it can be said that it is not the continued stimulus of the stellate and subpial cells that is preventing a second wave from propagating in the simulation of figure 17. As mentioned above, it is not clear whether the activity depression is also a feature of the true turtle cortex. However, if it is it seems highly unrealistic that even after 2 seconds the true cortex would be unable to respond to new stimulation.

It is believed that the cortical waves encode and carry with them visual information such as position and velocity. The visual distinction in the activity propagation patterns seen between the left and right waves already alludes to the possibility of spatial detection based on wave properties in the cortex model. To verify this model property, it has been shown that both an earlier version of the model that excluded subpial cells [21] and the later version described above [22] facilitate spatial distinction of stimuli based a principle component analysis done on the voltage potential data files used to generate the wave movies. Karhunen-Loeve Decomposition was used to translate the voltage potential files into a reduced three-dimensional beta space and detection was then done based on the resulting beta-strands of the waves.

2.5 Wave Analysis Techniques

The stored voltage potentials used to generate the pyramidal cell activity movies shown above represent a very high dimensional representation of a cortical wave. The human brain equips a human observer with the ability to make the analysis of the spatiotemporal dynamics of the cortex waves based on the visual inspection of the pyramidal activity movies. A much lower-dimensional wave representation is needed for efficient computational analysis with a computer. Karhunen-Loeve (KL) Decomposition (often referred to as 'Principle Component Analysis') is a standard mathematical technique used to reduce high dimensional spaces to a lower dimensional representation.

KL-decomposition and is applications to the model cortex voltage potential data will be discussed in section 2.5.1 on page 23.

Also, once the cortical waves are expressed in a computationally manageable way, a detection algorithm can be used to distinguish between wave produced from left and right LGN input based on a decision rule gained from statistics done on a set of training waves. The method used to gain a statistical decision rule based on the low dimensional wave representation and the effect of changing this method will also be discussed in sections 2.5.2 and 2.5.3.

2.5.1 Karhunen-Loeve (KL) Decomposition

The problem of finding a good representation of high dimensional data is a widespread and old problem. KL-decomposition was derived as early as 1907 to find an optimal sum-of-products approximation for measurable functions [24], and continues to be a widespread technique used to analyze complex data. One of the most common application areas is in analyzing video data. Robbins discusses KL-decomposition methods used in this context in detail in [24]. Here a brief summary of the basic method is presented. A detailed discussion of this the use of KL-decomposition to analyze the model cortex waves presented is given in various papers by Du [3] [4] [5].

A digital image is stored as a set of color or gray-scale values corresponding to locations in a pixel array. As such, a digital image can be thought of as an $N \times M$ matrix of pixel values, where N and M are the screen dimensions. Digital movies are simply sets of digital images or frames with corresponding pixels in a third time dimension. Thus, a digital video file can be thought of as an $N \times M \times T$ three-dimensional matrixes, where t, $0 \leq t < T$, is the time index of each frame. In this context each frame set of wave movie frames shown in the figures above is a series of two-dimensional slices from a single wave movie matrix. An $N \times M$ matrix can also be though of as a single point in an D dimensional vector space, where $D = N \times M$. Thus, a digital video file can be thought of as series of high dimensional vector-space points. If each frame has only three pixels, and thus each point is three dimensional, then a movie could be plotted as a series of three-dimensional points over time. Such a three-dimensional plot is not hard to visualize and would give an easily comparable plot representation of a three-pixel movie. However, digital images with a three-pixel resolution are not very practical. In order to visualize a higher dimensional frame as a single point its D dimensions must be reduced to three. The question is then what three dimensions should be used. It is hard to imagine being able to accurately represent a higher resolution digital image by any three of its pixels. In fact simply truncating the frame vector would cause a mean-squared error equal to the sum of the variance of the truncated pixels. Unless it is possible to rearrange the frame vector in such a way that the first three pixels represent a large percentage of the total gray-scale or color variance of the image and the rest of the pixels very little in value, which would of course be a very uninteresting image anyway, simple truncation of pixels can not give an accurate representation of the frame image. What is needed is a coordinate transformation from the pixel values to a representation in a new coordinate system of the image that contains the most important feature information in the first few dimensions. This can be done by exploiting the correlation between the values of neighboring pixels.

Let the frame vector be denoted as X and the vector representation of X in the new coordinate system be denoted as q. Then the projection, to be denoted as A, of X onto q is equal to the inner product of the vectors X and q. The projection equation is:

$$A = X^t q. \tag{2}$$

Since X^t is $D \times 1$ and q must be $1 \times D$ and A is a 1×1 matrix or singular value in the new coordinate system with D coordinates given by g. If the values of X are evenly distributed around a mean value (for a gray-scale image frame this means that there is on average as much black as there is white in the image so that the average pixel value is gray) then this mean value is the statistical expectation value of X. If this is the case, then, in order to make finding the best A easier, we can subtract the mean value from each X value so that the statistical expectation value becomes 0 without losing any frame descriptive information contained in X. If the expectation value of X is 0 then the expectation value of the projection A is also 0. The variance of a data set with an expectation value of 0 is equal to its means square value. So the variance v of A is equal to the expectation value of A^2. Using the definition of A, v is equal to the expectation value of $(X^t q)(X^t q)$, which can be written as $q^t R q$, where R is defined as the *correlation matrix* of X and is a $D \times D$ square matrix since X is a D dimensional vector. A detailed derivation of the correlation matrix is given in chapter 8.3 of [8].

The KL-decomposition method uses the fact that $q^t Rq$ is at an extreme when q is an eigenvector of R. Since R is a $D \times D$ matrix it has D eigenvalues corresponding to D eigenvectors. Since each eigenvalue represents an extreme in the variance, the corresponding A projections are often thought of as the *principal components* of X. Thus, there are D principle components for a given X. By taking each eigenvector to be a column in a total new coordinate set matrix the original coordinate set can be used in the projection equation stated above to calculate a vector a of principle components (i.e. $a = X^t Q$). This vector can be seen as an encoding of the vector X in terms of its most important features. What has been gained here is that the vector components of a correspond to eigen values of R and thus degrees of variance. Thus, the components of a are ordered in descending order according to variance. The desired coordinate system that contains the most important feature information in the first dimensions has been found. By truncating the last components of a only the least significant dimensions are eliminated. Hence, the truncated a can be re-projected onto X using Q to give the most accurate lower dimension estimate of X possible. The accuracy of this estimate depends on the extent of the correlation of the data set.

As discussed by Robbins, three principle components is generally enough to capture 75% of the information in video data and this is often sufficient to describe the behavior of a video data [24]. This is because neighboring pixels in video data are often highly correlated with each other. An example of an uncorrelated digital image would be a black and white snow image, such as what is seen on a TV screen when the signal is lost. In this case the value of each pixel is unrelated to the value of it neighboring pixels. However, in digital images without static distortion groups of pixels represent objects in the image and these objects highly correlate the values of the pixel that depict them.

A three-dimensional graph constructed from the first three principle components dimensions of a series of images, as suggested above, should have features distinctive enough to allow of video data analysis in this way.

2.5.2 Beta-strand Representation of Model Waves

At each simulation time step the voltage potential values of each model pyramidal neuron are written as a line in an output file. It is this file that is used to produce the wave movies seen above. While wave analysis could be done using the above-described technique on the movie images, a more direct approach is to view each line in the voltage potential file as a point in a high dimensional vector space with each pyramidal voltage potential serving as a coordinate value. Since there are in total 679 pyramidal cells in the model, each simulation time step vector has 679 dimensions. The cortex response over time can then be thought of as collection of vectors. This collection of vectors then represents a time window of the simulation response. When the window is large enough the entire wave response will be represented in the collections of time step vectors. Calculating an average correlation matrix over the entire time window will allow the principle component A coefficients to represent the principle features of the wave. Taking a second average over a set cortex responses will find the principle components of a set of waves. The first p A values can then be used to find pth order approximations of each time step vector according to the KL method described above. It has been shown by Nenadic et al that the 3rd order (p=3) approximation captures 99% of the response signal energy [21]. This is not unreasonable considering the high degree of correlation in the pyramidal voltage potentials. The nature of the wave response means that pyramidal voltage values are highly correlated with the voltage values of their neighboring cells.

Since the model cortex response has a random element (in Nenadic's case it was a random spatial redistribution of the pyramidal cells with each simulation while the spatial locations are fixed in the above model, so it is the random noise stimulation introduced to the pyramidal cells that gives a randomness to each response), the a vector of the first p A coefficients for each time step can be viewed as a vector random function. Statistical analysis of a random function can be facilitated by a second KL-decomposition on the a vectors of each movie. The average *covariance matrix*, which directly corresponds to the correlation matrix mentioned above, is then taken over each pth order representation a of each movie the set of movies. In this way a set of second KL-decomposition *beta*-coefficients b is found for each movie in the set and the qth representation of each movie is given by the first q beta coefficients. Thus, each movie can be represented as a point in the beta-space. Taking $q = 3$, each movie can be plotted as single a point on a three-dimensional plot. While, Nenadic showed that the beta points for movies of similar stimulus clustered together in beta-space this single point representation give no insight into the information content of the wave signal at different times.

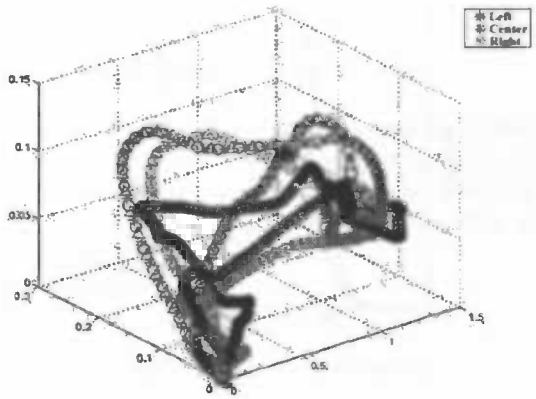

Figure 18: Plots of the average beta-stands produced from 100 left, center, and right input

By breaking each movie down into a series of successive submovies a beta-point can be found for a number of time sections and plotted in sequence to produce a *beta-strand* representation of a cortex movie that shows a progression over time. In fact the time window used to produce each beta-point can overlap to give a continuous beta-stand with as many beta-points as time steps in the simulation. Figure 18 shows the average beta strands of 100 left, 100 center, and 100 right input stimulus produced waves responses. The time window used was 10ms in width and was shifted 2ms for ever new beta-point [4] [5]. The total simulation time covered was 800ms. Thus each beta-strand contains approximately 400 beta-points (the actual number is <400 because the shifting was stopped when the end time of the window reached 799ms).

2.5.3 Beta-strand Detection of Model Waves

As has been repeatedly stressed in this paper that the cortical waves are believed to contain visual information is the propagation features. The idea behind using time windows to calculate the average correlations matrixes used to produce the beta-stand representations was that the beta points would then reflect the local features of the cortex response within the time window in which they were derived. Thus, the beta-stands reflect the change over time of the wave response, and thus the propagation properties. It should then be expected that the beta-strands could be used as a basis for input location detection. To do this the average beta-strands of groups of wave corresponding to different input locations of a test group are calculated as in figure 18 above.

Using these beta-strands as representative for their input location group, beta-strands produced from unknown stimuli can be compared against the representative strands. The unknown strand is then guessed to be a result of a stimulus from the same location as that of the group who's average beta-stand it most resembles. An easy measure of the resemblance of one beta-strand to another is to calculate the distance between corresponding beta-points along the strands and sum them over the beta-strand. This distance is taken to be the sum of the squares of the differences in the three principle beta dimensions.

By comparing the distances between the beta-points of the representative beta-stands over time it can be seen at witch time the distinction between the groups is greatest. Figuure 19 [4] [5] shows a plot of the differences between the left and center, right and center, and left and right average beta-stands in figure 18. Simply comparing the wave frames of a left and right wave in figure 15 show the largest visual difference at 200ms and 300ms and very little visual difference between the frames at 500ms and 600ms. Also, visual difference increases again in the frames at 700ms and 800ms. This pattern directly correlates with the plot of the left and right difference (green) in figure 19 and supports the claim that the beta-strands do indeed capture the characteristics of the waves.

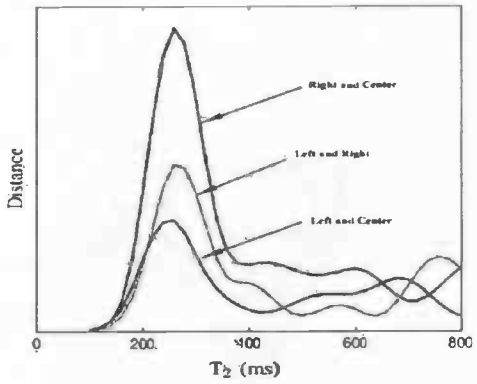

Figure 19: Plots of the distance between the left and center (blue), right and center (red), and left and right (green) average beta-strands over time.

Figure 19 also clearly shows that all three differences are greatest between 150ms and 250ms. Thus, it should be expected that time windows within this time span will contribute the most to the cumulative difference used for detection. The difference calculated only over this time period should be sufficient for detection. However, the waves do not die after 250ms and thus continue to provide information about the input stimulus.

Does the cortex process information transit over a short duration of time allowing the turtle to respond in several different ways to the wave information before it dies, or does information accumulated of the duration of the wave allowing the turtle one reaction based on a greater accumulation of information? By varying the time window over which the difference is summed, effects of different accumulations of wave information on detection can further be analyzed.

Two characteristically different window techniques can be used to represent the two information processing hypotheses above. A short sliding time window moved over the whole beta strand will show whether or not there is enough information throughout the durations of the wave to continually determine and respond to its position. An expanding time window can be used to see if the information captured in the time window does accumulate as the window size increases. The full results of this analysis along with an analysis of the effects of noise on detections are given by Du in [4] [5]. To include the effects of noise the three input locations were used to define a hypothesis space based on Bayesian statistics. The effects of noise were studied by comparing the effect of including the assumption of the presence of white versus colored noise in the statistics. The results showed the statistical approach to be better than the difference approach, described above, in both cases and the assumption of colored noise to be superior to the assumption of white noise. This is probably due to the fact that even white noise introduced to the pyramidal cells gives a colored noise effect on the activity patterns due to the stochastic nature of the pyramidal cell membranes captured in the model. The basics results of the windowing effects without the consideration of noise better demonstrate the information encoding limitations of the model, which are relevant to further discussion in this paper, and are briefly covered here.

As expected, both windowing techniques showed that the most information was captured in windows around 150ms in the simulation time. However, a sliding window of 100ms in size moved past 400ms the error probability of detection results increase sharply. At the end of the simulation time the error probability had reached 0.5. The expanding window preformed much better as later beta-points were included in the window. The error was shown to be negligible for windows starting form 0ms and ending up to 600ms. Once beta-points past 600ms were included the error probability did rise, but only to a small value of 0.05. Thus usable information does seem to accumulate throughout the cortex wave response, but smaller time windows only capture enough information to facilitate a transit response for the first 400ms. This evidence is not conclusive because the detection problem is a very simple one, only including three maximally varied input locations, and the detection results could worsen to the point of

a negligible difference between the sliding and expanding detection window techniques as spatial differences in considered input locations decreases.

2.6 Hebbian Learning with GENESIS

The GENESIS software provides a synaptic channel with Hebbian learning (hebbsynchan). The learning is implemented as a weight adjustment done on each synapse based on both pre and post-synaptic activity. A parameter that controls the speed at which the weight responds to activity changes (rate), a maximum and minimum weight value, and thresholds that limit the activity level at which learning takes place can all be specified.

2.6.1 The Basic Learning Rule Equation

The basic equation is

$$change = rate * dt * (pre * post), \tag{3}$$

where *rate* is the factor that controls the learning speed, dt is the channel simulation clock rate, and *pre* and *post* are measures of the pre (originating cell) and post (receiving cell) synaptic activity. The post-synaptic activity is taken to be difference between the nearest threshold and the average voltage potential of the receiving cells. Since each cell-to-cell connection has its own synaptic channel in the model, there is only one receiving cell and thus the average is taken over only one post-synaptic activity. The pre-synaptic activity is calculated for each synapse of the channel and is the difference between the nearest threshold and the pre-activity of the synapse. However, since there is only one synapse per channel in the model, there is only one pre-activity value per channel also. Thus, the learning is based simply on the activity level of the originating and the receiving cell of each connection.

The initially calculated change is checked against a max change, which is simple the difference between the maximum weight limit and the minimum weight limit. After the final weight change value is calculated it is simply added to the previous weight with the equation:

$$weight + weight + change * scale, \tag{4}$$

where *scale* is a smoothing factor based on the distance to the nearest weight boundary which allows for a gradual boundary approach. Boundary checks against maximum and minimum weight values are then done. GENESIS forces the obvious lower limit of zero because negative weights lose any biological basis. However, because weight equation 4 is additive and not multiplicative, the lower bound can be zero. A zero weight connection models a dead synapse, which cuts off communication between its pre and post-synaptic cells, but it can come back to life when its pre and post-synaptic cells again become active. However, a cell in the cortex model that has been completely cut off from the cortex will not be able to reconnect if it is not directly connected to the layer of input LGN cells.

2.6.2 The role of Activity Thresholds

As alluded to above, synaptic activity thresholds can be set to define what is considered high and low activity. Both high and low thresholds can be set for both pre and post-synaptic activity. In this situation the 'nearest' threshold mentioned above is the high threshold when activity is above the high threshold and the low threshold when activity is below the low threshold. When the activity level lies between the thresholds, checks insure that no learning takes place and *change* is set to 0. An extra check is needed to assure that no learning takes place when both pre and post-synaptic activity levels are below their respective lower thresholds. The influence of the thresholds can be analyzed by considering learning regions in a threshold space as depicted in figure 20. The areas of no learning allow for a base noise level of activity to be determined and ignored by the learning function. This assures that learning will only take place in response to raised or lowered activity levels resulting from an input stimulus.

It can be seen from the threshold space diagram that there are three areas of learning in the basic threshold situation. According to Hebb's original idea of learning, weight strengthening occurs in the region above both the pre and post-synaptic high thresholds. Accordingly the two regions in the upper right and lower left corners, where the pre and post-synaptic activity levels most oppose each other, can be seen as implementing Hebbian Decay.

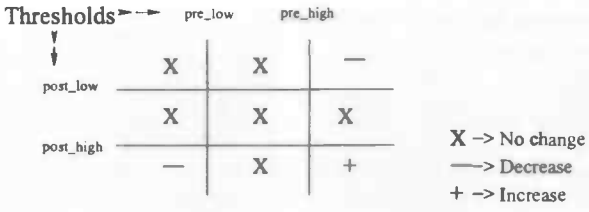

Figure 20: Threshold situation reflecting simple Hebbian learning with Decay

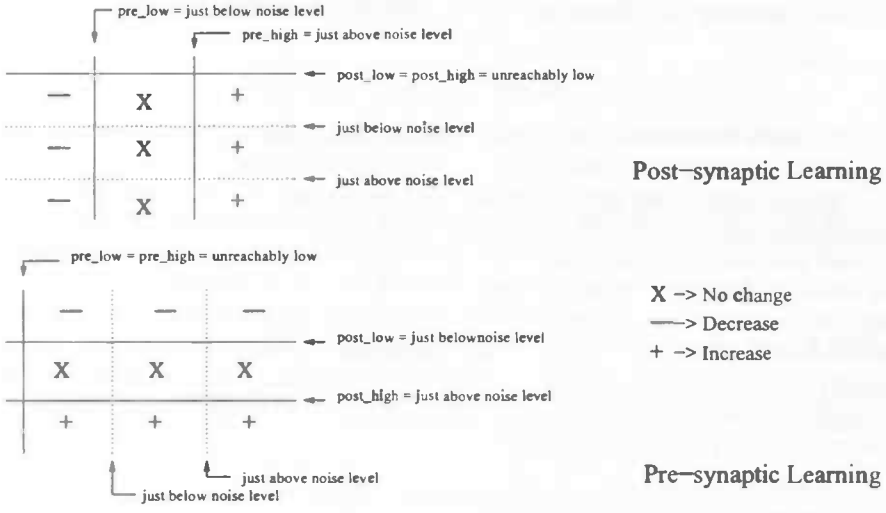

Figure 21: Diagram showing the pre and post synaptic learning schemes

The threshold levels can also be used to implement two unique learning schemes. By setting both the high and low threshold values to unreachably low values either pre or post-synaptic activity levels can be allowed to have control over the learning. When the pre-synaptic threshold values are set to levels that ensure the values in the model will always be above them whether or not the weights increase or decrease will be solely governed by the post-synaptic activity levels and if the situation is flipped the pre-synaptic activity levels will govern the learning. It should be noted however that the magnitude of the weight change is dependent on the magnitudes of differences between the activity levels and the nearest threshold value. Thus, both pre and post-synaptic activity levels will always have an effect on the learning. Both the pre and post-synaptic learning cases are depicted in figure 21.

Both the pre and post-synaptic learning schemes skew the idea of Hebbian learning. Hebb asserts that it is simultaneous and opposing activity of both source and destination cells that govern strengthening and decay. As can be seen from figure 21, when one side of the synaptic channel is defined as active even when it is at an inactive activity level one of the two regions of Hebbian Decay defined above will become a region of Hebbian strengthening. Also, the region of no learning when both cells are inactive becomes a region of decay. However, the influence of both of these regions is limited by the difference between the unreachably low level and the actual low activity level. As this term approaches zero the influence of the governing term approaches zero.

Post-synaptic learning can be thought of a responsive learning because input only indirectly leads to changes in

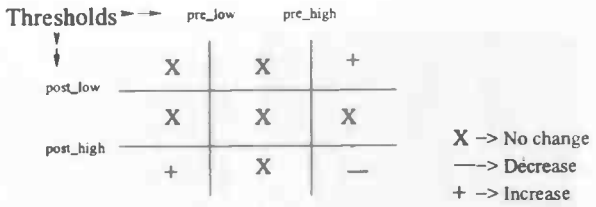

Figure 22: Diagram showing anti-Hebbian (learning rate = -x) threshold relationship to the weight change

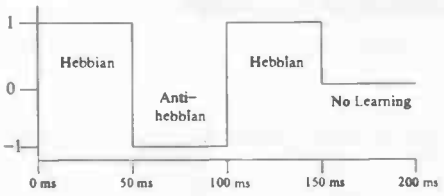

Figure 23: Using a pulse signal to control the learning rate

the weights. The activity levels of the pyramidal cells at the destination end of the connections must first respond to the input before the connection weight values can. However, in the case of the pyramidal, stellate, and subpial cells, which are directly stimulated by the LGN cells, pre-synaptic activity driven learning allows for a direct weight response to input. Both of these learning schemes and ways in which they can be used and mixed to shape the learned weight response will be discussed below.

2.6.3 The Role of the Learning Rate

The most crucial parameter when determining the basic type of reaction the model will have to the activity wave, is the *rate*. By controlling the rate, the cortex learning can be made short-term, long-term, or even anti-Hebbian. Short-term learning will adjust quickly to the input at hand, while long-term learning requires a history of input to fully adapt to the input. As can be seen in equation 1 and 2, a negative *rate* will simply reverse the effects of the learning and lead to the change space diagram below in figure 22. Obviously, this depicts the anti-Hebbian situation.

The rate can also be varied as a function of time. GENESIS allows for the rate to be coupled to a time varying function such as a sine wave. The rate is simply multiplied by the value of this function at each time step before it is used to calculate the change. By using the GENESIS block pulse function generator to generate a series of pulses based at -1 or 0 and of height 0 or 1, as depicted in figure 23, the rate can be made positive, negative or zero. Thus, the channel can switched off and flipped between Hebbian and anti-Hebbian learning as function of simulation time.

3 Results

Even though the Hebbian-learning rule is quite simple, letting it loose on a complex model such as the cortex model can produce complex results that are hard to analyze. Thus, full Hebbian learning implemented on all synaptic connections is not handled in this paper. This section focuses on using Hebbian learning in specific ways to address specific features of the cortex model. In order to visualize the effects of learning on the weights, a weight movie, similar to the activation movies is made.

An example of one of these movies showing the pyramidal-to-pyramidal connections with its corresponding activation movie is shown in figure 24. The warmer colors indicate higher weights and the cooler colors indicate

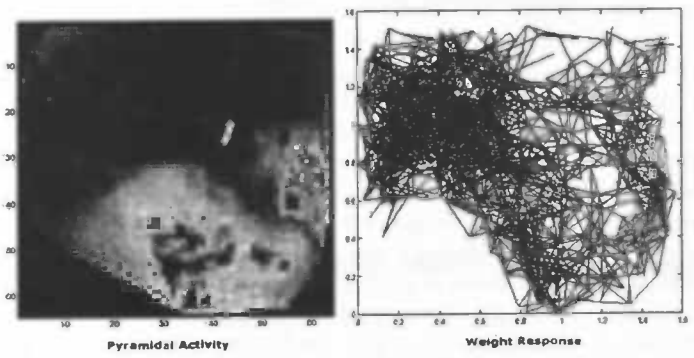

Figure 24: Hebbian weights and the corresponding cortex activity

weaker weights with black indicating a zero weight. Here the effects of Hebbian learning in response to the activation levels of the pyramidal cells, with the use of the threshold values mentioned above to prevent learning at noise activity levels, can be seen.

3.1 Using Pre-synaptic Controlled Learning to Compensate for the Input Bias

As mentioned the cortex model expresses a small bias between left and right input based on the discrepancy of LGN axon varicosity densities. The less dense area covered by the axons of the right most LGN cells leads to the necessity of a slightly stronger stimulus pulse to produce activity needed for the pyramidal response activity to become self propagating. This section suggests a LGN axon learning mechanism for compensating for this bias.

Recalling that the model implements synaptic channels between LGN neurons and pyramidal neurons in the sphere of influence of each varicosity point along each LGN axon, increasing the weights of the LGN-to-pyramidal cell connections will increase the strength of the influence of the input. In this way the influence of the right-most LGN cells on the pyramidal cells can be increased by increasing the weights of their connections with the connected pyramidal cells. This could be implemented directly with stronger fixed weights on connections from the right LGN cells then from the left LGN cells. However, the magnitude of this strength increase would need to be directly proportional to the bias of each LGN neuron and this is difficult to determine. A simpler method is to allow each LGN-to-pyramidal connection to 'sense' the strength need to elicited the sufficient pyramidal response and adjust it weight accordingly. Thus, when the destination pyramidal is not responding to the LGN stimulation the weight should be increased. This describes the anti-Hebbian learning situation.

Taking the basic post-synaptic learning scheme presented above and raising only the high pre-synaptic activity threshold to reachable levels allows for the post-synaptic activity levels to determine the direction of the learning but blocks any learning below the high pre-synaptic threshold. If the high pre-synaptic threshold value is set to a level just below the spiking activation level of the source neuron, as depicted in figure 25, learning will only takes place when the source neuron is firing. Just as in the basic pre and post-synaptic learning schemes, this learning scheme still somewhat skews the Hebbian idea of learning reflecting synchronized activity. Figure 25 clearly shows that the low pre-synaptic/high post-synaptic half of the Hebbian Decay region is blocked. However this is just what is needed the implement the bias adaptation described above when the learning rate is set to be negative as also shown in figure 25.

With this learning scheme the weights of the connections between the active LGN cells and their influenced pyramidal cells will increase when the pyramidal cells are not being fired and have low activity levels, as shown in the upper left right corner of the threshold-space plot in figure 25. Once the pyramidal cells begin to fire their activity levels will be high and the weights will decrease, as shown in the bottom right corner of the threshold-space. If the high post-synaptic threshold is high enough to prevent the weights decreasing before pyramidal activity is self-

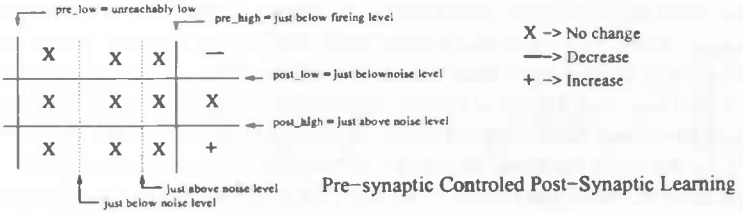

Figure 25: Threshold situation for learning only when source neuron is active

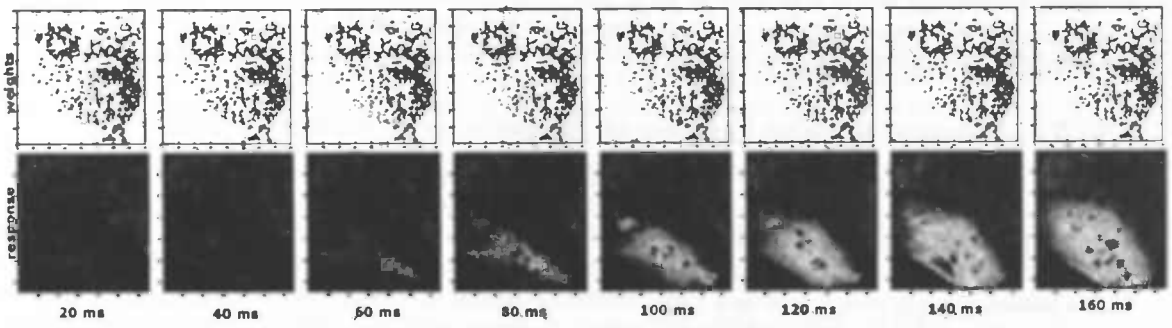

Figure 26: LGN synaptic Hebbian learning weight and pyramidal activity reaction at 20, 40, 60, 80, 100, 120, and 140 ms

sustaining then once the weights begin to decrease the self-propagation phase will already have been reached. Due to the bias, less weight strengthening will produce a self-sustaining level of pyramidal activity when dealing with the left LGN neurons as apposed to the right LGN neurons. However, in both cases the input will be strengthening to the point of triggering a wave response. Thus the bias will reflected in the LGN-to-pyramidal connection weight response and not the pyramidal activity response.

The results of implementing this learning scheme in responds to a 150ms 2.0 pA right input pulse can be seen in figure 26. Here the LGN-to-pyramidal connections are shown as originating from the varicosity points to simplify the picture. However, connections where still implemented as direct LGN-to-pyramidal connections as described above.

First, it is clear form figure 26 that the weights do indeed increase to the point of allowing wave propagation despite the fact the input pulse is only a quarter of the minimum strength mentioned above. Further, it can be seen that the weights return to their original low values before the time of the end of the LGN input pulse. At this point the LGN cell activity levels decrease until they are again below the pre-synaptic threshold. It can also be seen from the figure that pre-synaptic activity constraint allows only the connections from the stimulated right LGN cells to respond to their target pyramidal activation levels. Thus, as shown by the last frame, once the activity becomes self propagating there is no lasting trace of the weight compensation. If the pre-synaptic activity levels of all LGN cells are low enough to prevent further learning once the wave has moved on and died then the weights are left in the their initial state and following input will not be influenced by the preceding LGN weight compensation. Unfortunately, in the cortex model, the stimulated LGN cells remained at a high activity level relatively long after the end of the input pulse. This allows the LGN-to-pyramidal weights in the wave origin to be driven back up to their maximum level by the activity depression once the wave has moved away from the origin. However, it can be seen from

figure 26 that the origin has already become self-sustaining at 100 ms. The input could be removed at this point. This would give the LGN activity levels more time to die down to below the pre-synaptic threshold level before the wave leaves the origin. Thus, only input that is persistent after a wave has been triggered will cause the weights to be left in favorable state to further input from the same input location. This could be seen as both undesirable and desirable feature. Either way, this feature is interesting when considering wave information encoding applications.

However, it should be noted that the right moment to stop the input to prevent the above described learned weight reminisce depends on the input location, which in a sense introduces a new input bias. As seen in figure 17, the persistence of input after the wave has moved away from the origin area will not trigger another wave, but will hold the input stimulated pyramidal cells at a higher activity level. Therefore, the activity depression will not be able to drive the LGN-to-pyramidal weights back up as long as the input is present. It is the fact that the activity depression drive the activity levels of the pyramidal cells down much faster then the LGN activity dissipation rate of the LGN cells causes the weights of the directly input stimulated cells to again increase. A practical way to prevent this is to force the learning to stop once the input has stopped by using the block pulse function method presented above to control the learning rate as a function of time. The synaptic channels can be coupled with a block with a base magnitude of 0 and peak magnitude of -1 that corresponds in length to the length of the LGN input pulse. Doing this couples anti-Hebbian learning to the presence of input and no learning to the absence of input.

3.2 The Effects of Hebbian Learning on the Behavior of the Cortex Model

As seen in figure 16, the cortex activity wave response is cyclic in nature. Because the learning is solely based on the activity levels of the cells the learned weight response must also be cyclic in nature. Thus, no real steady state will be reached unless learning is stopped or the cortex reaches a steady activity level. However, the cortex must remain responsive to input in order to function and thus should never reach a steady activation state while input is present. In this context a steady state would be a cyclic change in weights in response to input that always returned to the original weight values after the propagation of a wave. However, the response of the cortex is not perfectly cyclic. As discussed above, an activity wave is followed by an activity depression that leaves the cortex in a lower activity state after a wave then where it began. Hebbian learning will cause the weights to be driven down in response to the activity depression. A lower weight boundary can be set to stop the weights from lowering past their original values. In this way a limit-cycle behavior weight response would be reached. However, the activity depression will prevent further waves from propagating.

3.3 Overcoming the Depression with Anti-Hebbian learning

Considering the situation described above where a wave has propagated leaving a activity depression behind and the weights have returned to their initial values, it is clear that not much has been gained through learning. What is needed is a learned weight response to the activity depression that compensates for the lowered activity levels. In this situation the weights would be in a state where pyramidal to pyramidal connections weights are high and inhibitory to pyramidal weights are low in response to low activity. Thus, anti-Hebbian learning is required on pyramidal to pyramidal connections, while inhibitory to pyramidal connections can use Hebbian learning. This situation is depicted in figure 27. In this way the activity depression following a wave will serve the function of driving the weights of the connections that work to stimulate cortex activity up and those which work to prevent and kill activity down.

The movies reflect the voltage potential levels of the pyramidal neurons. Thus, the activity depression seen in the movies is solely an artifact of the activity levels of pyramidal neurons. Since it is this depression that is to be compensated for the learning should be reactive to the activity levels of pyramidal neurons. Because learning is implemented only on connections going to pyramidal neurons, it is the post-synaptic activity levels that should control how the weights rise and fall. Accordingly, the synaptic channels in the model with pyramidal cells as their destination cell where implemented as GENESIS Hebbian synaptic channels with activity thresholds set according to the post-synaptic learning scheme described in section 2.6.2. The learning rate of the Hebbian channels with inhibitory source neurons was set to 10.0 while the learning rate of the Hebbian channels with pyramidal source neurons was set to -10.0 implementing anti-Hebbian learning.

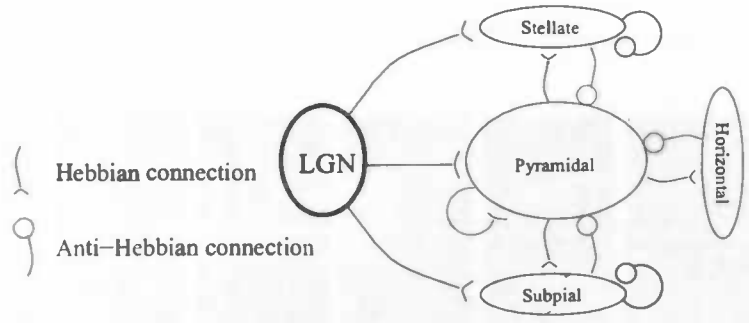

Figure 27: Anti-Hebbian/Hebbian learning situation

It has been shown that using the anti-Hebbian/Hebbian learning combination described above can lead to follow up waves in the cortex model that overcome the activity depression and propagate. The cortex was given six consecutive right input pulses 8.0 pA in strength 400ms apart which resulted in six consecutive activity waves. 8 frames of the activity movie corresponding to the model response to four consecutive right inputs can be view in figure 28.

A frame just before and after the beginning of the sixth wave and the corresponding weight frames can be seen in figure 29. The situation just before the sixth consecutive input shows that the pyramidal to pyramidal weights in the area of the depression have been driven to their maximums (represented by their red color). It can be seen from the situation just after the second input that the weights responded to the second wave activity by decreasing and the inhibitory to pyramidal weights increase to control the wave.

The weight response is clearly cyclical, but does it reach a limit-cycle as described above?

It can be seen in figure 28 that after several consecutive wave propagations the activity depression covers the majority of the cortex. The weights react accordingly by being driven to their maximal values in the anti-Hebbian case and minimal values in the Hebbian case. The learning allows the weights to shift to the opposing extremes in response to high activity of a following wave. In this way the weights cycle between the extreme limits as the wave propagates. Thus, a steady weight change state, or limit-cycle behavior, has been reached. The plots of the average weight values over time of all outgoing pyramidal to pyramidal cell connections of several pyramidal cells and all outgoing horizontal to pyramidal connections of several horizontal cells are show below in figure 30.

The plots show that the oscillations of the pyramidal to pyramidal connections and the horizontal to pyramidal connections oppose each other and stabilize after 5 oscillations. The stellate-to-pyramidal and subpial-to-pyramidal connections also stabilize. However, they oscillate only slightly above zero at their stable state. This is an important factor in the compensation of the activity depression. Since the stellate and subpial cells are stimulated along with the pyramidal cells by LGN input, they act preemptively to inhibit the stimulated pyramidal cells and maintain the balance needed to form an activity wave. However, the pyramidal activity levels have already been lowered by the activity depression following propagation when the secondary stimuli are applied. Thus, the pyramidal cells are effectively already preemptively inhibited when secondary stimuli are applied and the preemptive inhibition of the stellate and subpial cells is not needed. When the weights of the stellate and subpial to pyramidal connections remain high in the preemptive phase of secondary waves the stimulus is not able to overcome the depression and triggers no wave propagation. Once the wave begins to propagate the stellate and subpial cells provide responsive inhibition, just as the horizontal cells do. This accounts for the presence of small oscillations at their limit-cycle.

The subpial cells respond very quickly to stimuli and therefore play the largest role in preemptively inhibition. As discussed above, it is for this reason that subpial cells are the main cause of the input location bias that exist due to their uneven spatial distribution. When activity levels are very low, this bias is increased. As a result when subpial to pyramidal weights are not driven to zero by the activity depression after several successive waves, input from the right or center is less likely to result in a wave. However, the bias is eliminated in the situation depicted by the plots in figure 30.

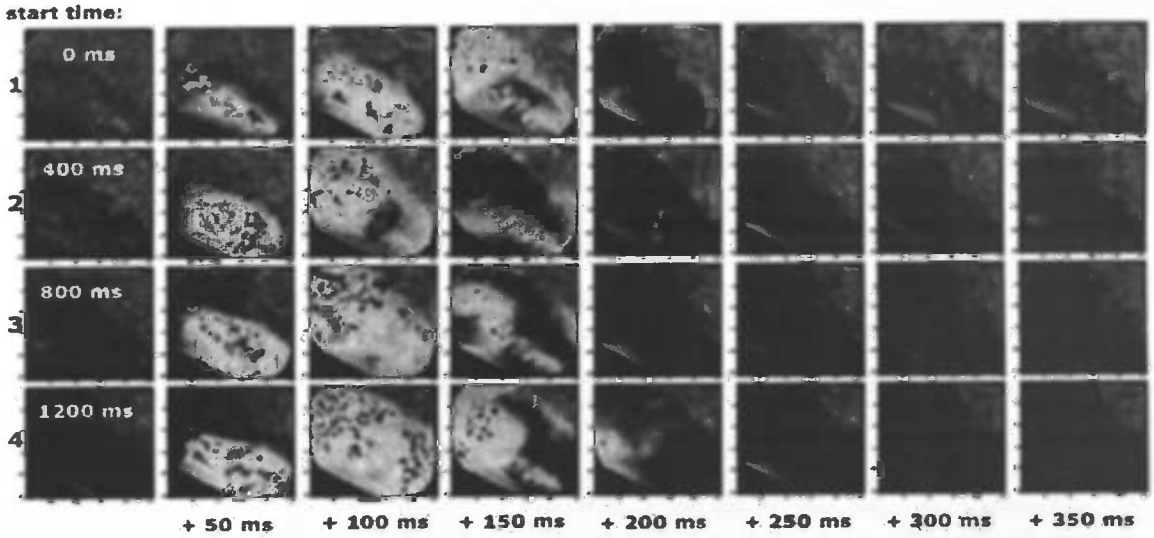

Figure 28: 8 frames of 4 waves at 1, 400, 800, 1200 from time 1-1550ms showing followup waves

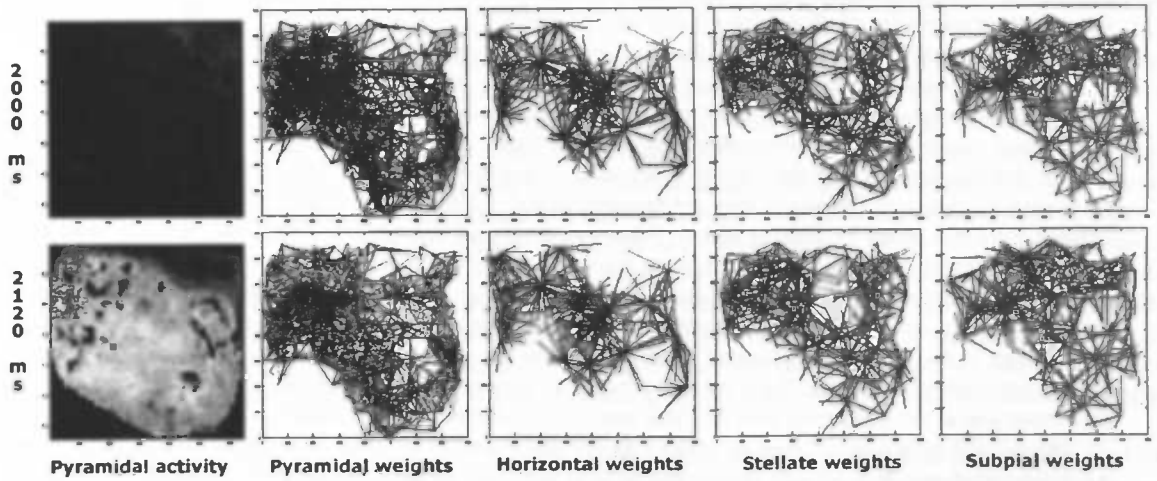

Figure 29: Hebbian and anti-Hebbian weights and the corresponding cortex activity

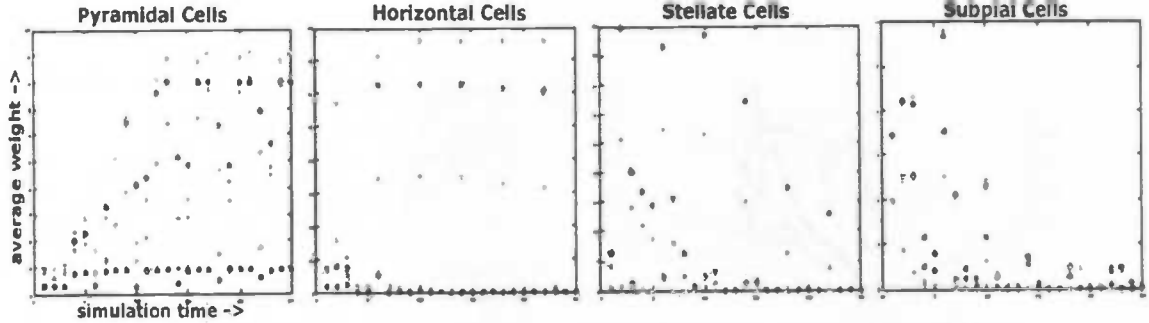

Figure 30: Average weight of all outgoing connections from four pyramidal, horizontal, stellate, and subpial cells. Each of the four colors in each plot represent one of the four cells taken from different regions of the model space. The weights are plotted over simulation time

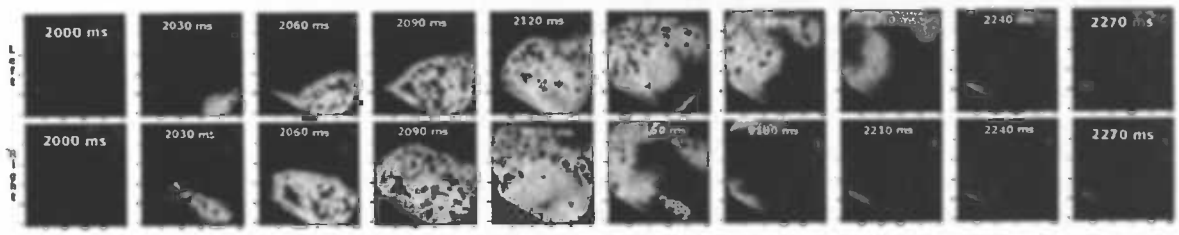

Figure 31: 10 frames of the 6th left (top) and right (bottom) waves (at time 2000ms,2030ms, 2060ms, 2090ms, 2120ms, 2150ms, 2180ms, 2210ms, 2240ms, and 2270ms)

3.3.1 Position Delectability of Secondary Waves

The fact that secondary waves can be produced through learning is a significant finding. However, these waves are visibly different and propagate faster then primary waves without learning. A very important aspect of the cortex waves is the assumption that they contain information about the visual scene and consequently a very important feature of the simulated waves is the ability to do spatial detection on the visual input based on there propagation characteristics. In this context that fact that the wave characteristics change using learning is significant.

However, even in the follow-up waves, visual differences remain between waves caused by left and right stimuli. Although the follow-up waves propagate and reach the caudal pole of the cortex faster than waves without learning, the input stimuli location still plays a large role in determining the propagation speed. As can be seen from figure 13, the axons from LGN cells located on the right side of the LGN space extend toward the caudal pole. Thus, input from the right stimulates pyramidal cells much closer to the caudal pole then input from the middle or left causing the resulting waves to reach the caudal pole faster. LGN axon distribution is the main cause of the difference in wave characteristics that allows for input distinction based on the waves. Of course weight-learning does not effect this spatial distinction. The fact that the speedup produced by the described learning scheme is roughly constant for both left and right input waves preserves the difference in propagation speeds. This can been seen in the left and right waves of figure 31. Thus, it should be expected that spatial distinction, and consequently detection, should also be able to be done on these waves.

In order to prove that the characteristic of wave distinction based on input location remained sufficient to allow for spatial detection 20 right and 20 left 6th waves were produced. Here '6th waves' refers to the wave produced by the sixth consecutive input stimuli of one simulation. For both left and right 20 different variations of left right

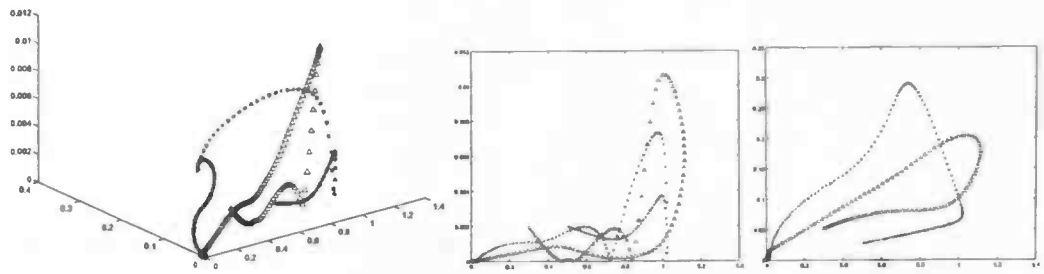

Figure 32: Plot of the average beta-stands of the left waves in red and right waves in blue

and middle input locations of the first 5 inputs were used to produce five preceding wave propagations. This was done to show independence of preceding wave activity once the steady weight reaction state has been reached. Just as above, the LGN cells were stimulated with 150ms block pulses every 400ms starting at 0ms. Thus, the sixth stimulus was presented at 2000ms. As can be seen from figure 31, the sixth waves have reached the caudal pole and died within 300ms. Thus, the cortex reaction from 2000ms to 2300ms was used to produce three-dimensional beta-space representations using KL-decomposition as described in section 2.5 on page 22. The average beta stands of the left and right waves are shown in figure 32.

Both the left and right wave produced average beta-stands that reflect the cyclic build up and regression of activity that characterizes the wave response. However, there is clearly a difference in the general characteristics of each cycle. The two main distinguishing features between the two beta-strands are emphasized in the second and third plots of figure 32. Each of these plots is a 2-D cross section of the 3-D beta-coefficient space. The first cross-section along the 1st and 2nd beta-coefficients axis shows the right beta-stand take a very direct out and back path. The left beta-strand, on the other hand, makes a much broader cycle that seems to stall as it makes its turn back to the origin. The second cross section along the 1st and 3rd beta-coefficient axis shows two small peaks dominated by one central high peak along the path of the right beta-strand. The left beta-strand however has a much less dominant central peak and more prominent peripheral peaks.

Looking again at the sixth wave frames above the two main distinguishing beta-strand features directly parallel the two main distinguishing features between the left and right waves, namely that the right wave is much more violent and direct its activity explosion and regression, while the left wave builds up more slowly and moves in a smaller more compact activity ball from the rostral to the caudal pole. Thus, learning does not seem to have prevented the beta-strand technique from capturing the two main distinguishing characteristics. From this it should be expect that the visual detection between right and left waves should be possible to reproduce computationally.

To prove this 20 additional simulations using different first four input locations for 10 left sixth inputs and 10 right sixth inputs were run. However, this time the input position of the fifth stimulus was opposing to that of the last stimulus. This was done make sure that the sixth wave is not heavily influenced by the preceding input. The beta-strands produces from the sixth waves of these simulations can be seen in figure 33. Each plot in figure 33 show a pair beta-stands from one left and one right wave. It can be seen that the left and right beta-strands in each of these pairs that the left beta path is consistently broader while the peak in the right beta path is consistently higher and sharper.

The original 40 beta stands were used as the training set to produce Bayesian statistics for detection on the beta-stands of the additional 20 sixth waves. The optimum *Expanding Detection Window* (EDW) technique that assumes colored noise in the response signal reported by Du to be the most optimal [4] [5] was used. The results are shown in figure 34.

The first seven plots show the classification of each of the 20 beta-stands into two groups based on detection windows including the first 5, 10 15, 20, 25, 30, and 35 beta points respectively. During training group one was known to be the beta-strands generated from the set of right sixth wave, while group two was that of the left. The

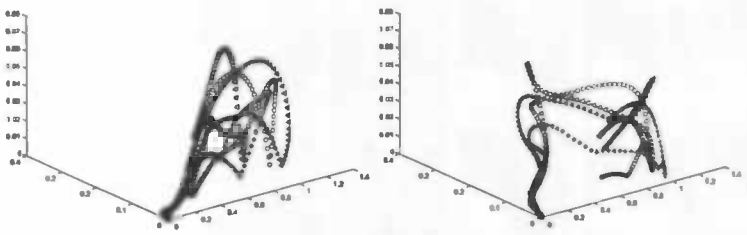

Figure 33: Corresponding left (1-10) and right (11-20) beta-stands of the test group

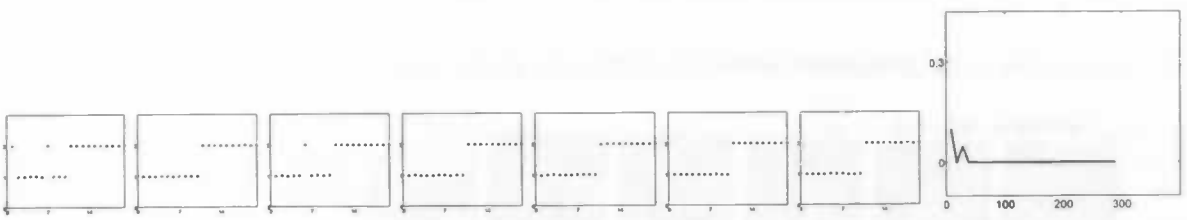

Figure 34: Detection results of the 20 test waves. (plots 1-7) Hypothesis categorization of using expanding times widows of size 5, 10, 15, 20, 25, 30, and 35 respectively. Points 1-10 correspond the beta-stands of the left test data set. Points 11-20 correspond the beta-stands of the right test data set. (plot 8) Error probability plotted in increasing time window size

first 10 beta-strands of the test set were generated from 10 left sixth waves and the last ten were generated from ten right sixth waves. The results of the detection parallel those for EDW using the colored noise assumption presented in Du's work. Once the size of the detection window increases past 20 beta-points, corresponding to 40 ms in the simulation time the error probability decreased to zero and, as shown by the eight plot of the error probability over window sizes up to 290 ms, did not increase again thought the length of the wave strands. It should be expected that since only two hypotheses are used in the detection statistics, the results should be at least as good as those presented by Du for three hypotheses if the speedup has not degraded the information content of the wave. This is shown to be the case.

Figure 35 shows the differences between the average beta-strands in figure 33 plotted over simulation time. As discussed in section 2.5.3 on page 25, the best detection results can be expected in time windows where the difference between left and right beta-strands is largest. From comparing figure 35 to figure 19 it can be seen that the two peaks in the left and right difference plot of non-learning waves have been intensified and squeezed into the shorter time frame of the learning waves. This is a consequence of the increased difference between the non-active and active pyramidal voltage levels during learning wave propagation. The second peak, which is caused by the fact that the right wave die faster than the left waves, and is relatively small and late in the non-learning plot is especially magnified. In fact the second peak in the non-learning plot can be said to be too small and too late to be within the high information content time window. However, in the learning wave case, the second peak is almost as prominent as the first peak and the time gap between the two is short. A detection window size larger then 40 ms should always include enough of both peaks to allow for good detection results even when using the sliding detection window techniques discussed in section 2.5.3 on page 25. Thus, is can be argued that the window of high information content includes both peaks, and is thus approximately 200 ms wide, in the learning case. In the non-learning situation this window is also approximately 200 ms wide. This suggests that the information content is not diminished through learning. The information is merely compressed. However, it should be realized that the difference between the right and center waves did not show a significant second peak in figure 19 as the left and

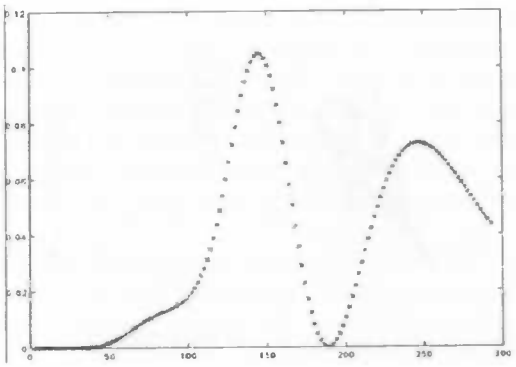

Figure 35: Difference between average left and right beta-strands plotted over simulation time

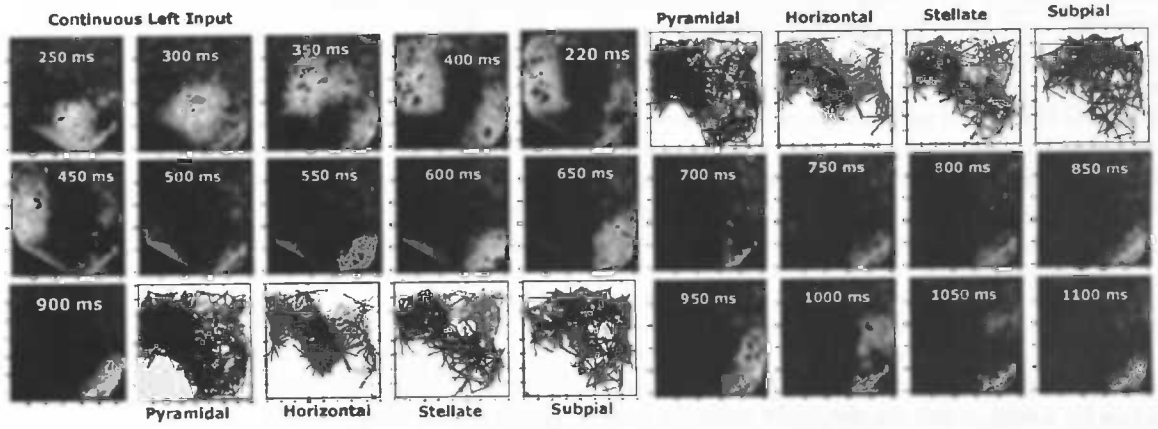

Figure 36: Cortex reaction to a continuous left stimulus

right and left and center differences did. It was not determined if the initial much larger difference between right and center waves in sufficient to make the same information compression argument in this case.

3.4 Responding to continuous stimulus

As previously noted, without learning the model cortex only responds to continuous stimulus with one initial wave despite the continued presence of input stimulus. Review of the stimulation movie in figure 17 shows flashes of activity in the area covered by the stimulated LGN axons after the initial wave has died. From the results already seen using the Anti-Hebbian/Hebbian learning scheme discussed above, it should be expected that these flashes would result in follow-up waves when the weights are allowed to learn in a similar manner.

However, using the same post-synaptic learning scheme as above with a continuous left stimulus produces results very similar to the no learning situation. As can be seen in the frames of figure 36, the cortex responds with one initial left wave followed by activity flashes. Just as in the case with no learning these flashes die before they are able to propagate. Hence, learning seems to accomplish nothing in the continuous stimulus

The weight situation during the propagation of the initial wave (at 420 ms) is also shown in figure 36. It can be seen that the weights are responding to the activity just as should be expected. The weights in areas of high activity are unfavorable to propagation and the activity depression following the wave has driven to weights in this area to

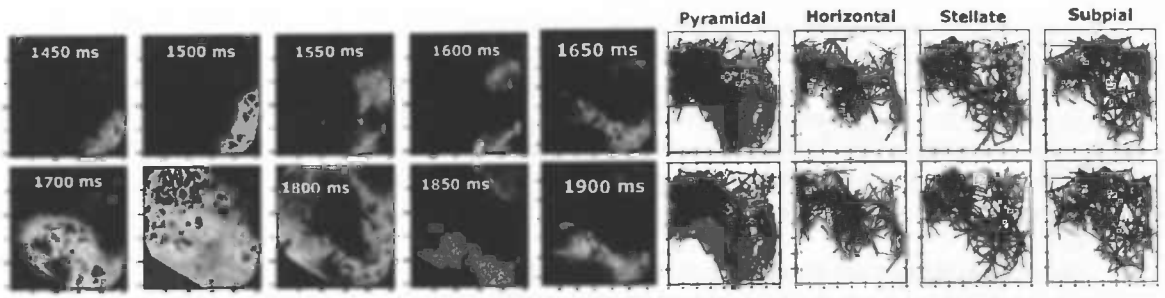

Figure 37: Cortex reaction to continous right stimulous directly following 1600ms of continuous left stimulous

a favorable state. However, the continued presence of stimulus seems to be preventing the activity depression from covering the area of the wave origin.

Examination of the weight situation after the propagation of the wave, as shown in the weight frames of figure 36 at 900 ms, shows that the cells continuously stimulated by the left stimulus have become isolated in an area of unfavorable weights that prevents them from exciting cells in the area of favorable weights. This explains the lack of a second left wave after the propagation of the first one. The excited pyramidal cells in the origin area are able to stimulate surrounding pyramidal cells to produce the activity flashes because the activity levels of the destination cells of connections leaving the origin area are low and Anti-Hebbian learning is used. The connections from the pyramidal cells leading back into the active origin area are weak because there destination cell activities are high. However, the connections from the inhibitory cells leading back into the active origin area use Hebbian learning and are strong due to the higher activity of their destination cells. In this way the flashes of activity do not serve to restimulate the origin area but, in fact, inhibit it. Thus, the origin activity is not able to build up to the point of expansion, as seen in the wave of figure 15, and the activity again subsides.

If the stimulus were to be removed after the initial wave begins to propagate, as in the above simulations, the activity depression should cover the origin and drive the weights to their favorable state. Thus, when the stimulus is reapplied the weights in the origin area will be in a favorable position and the activity will be able to build to the point of propagation before the inhibitory cells react to kill the origin activity.

What if the stimulus was not removed, but simply moved to a new LGN location?

The same simulation that showed no follow-up wave for 1100ms after the propagation of the initial left wave discussed above demonstrates that when the stimulus is switched to the right location at 1600 ms, a right wave is produced despite the presence of the activity depression. Figure 37 shows the cortex response from 1600 ms to 1900 ms of this simulation. As can be seen from the weight state shown at 900 ms in figure 37, when the stimulus location is moved, the origin of activity is moved to a cortex area that has been driven to a favorable state by the activity depression. Thus, the origin activity will be able to build to the point of propagation before the inhibitory cells react. The frames after 1600 ms confirm this by showing a wave of propagation with right wave visible propagation characteristics.

The weight state shown at 1900 ms indicates that isolation effect is consistent and the right activity origin has been held in an unfavorable state after the right wave has propagated.

This is an improvement over the non-learning situation. Without learning the cortex becomes 'numb' to any further stimulation after the propagation of an initial wave independent of the following stimulus situation. A long absence in stimulus is needed to let the pyramidal activity levels recover form the weight depression without learning, while only a change in input location or short absence of stimulus is required to allow for follow-up wave propagation with the described learning scheme. In fact, input feature based numbing is not an unrealistic cortex feature.

It is widely observed feature of visual cortices that they respond better to a moving object then to a stationary one. In fact it has been shown that eliminating the tiny movements called microsaccades that humans eyes make to keep the visual stimulus constantly changing results in temporary blindness [10]. The above results show this

stationary stimulus numbing to be reflected in the cortex model when the above learning scheme is applied. In mammalian type cortices that show direct mapping of retina stimulus location to the location of the cortex activity, numbing is often explained as a cellular characteristic. When certain areas of a cortex responsed to specific visual stimuli features, such as location, numbing of the cells in those areas only numbs the cortex to that feature responded to by that area of the cortex. However, it is shown in the model that, due to the wave response of the turtle cortex, the resulting activity depression is global enough to numb the model to stimuli from all visual field locations. Yet the learning weight compensation *is* shown to re-localized the numbing to the specific stimuli location origin areas of the cortex.

While observing spatially localized numbing after only one initial wave propagation in the model cortex may be simplifying things too much, the discussed unfavorable weight localization around the continuously stimulated area does suggest a possible mechanism for the numbing in real cortices that exhibit a wave response.

3.5 Returning to the initial weight state

While it has been shown that learning can compensate for the activity depression, the issue of returning to the initial weight state once the input has been absent sufficiently long to allow the activity state of the pyramidal neurons to recover from the activity depression has not yet been addressed. After a sufficient number of consecutive wave propagations the weight change reaches limit-cycle behavior as discussed above. In this state the anti-Hebbian connections are driven to the minimal values after the propagation of each wave while the Hebbian connection are driven to their maximal values. Given the Hebbian learning scheme as it is implemented in standard GENESIS, the weights will not return to there initial values once the input has stopped long enough for the activity levels to recover. As seen in figure 20, when the activity is below both the low pre and post-synaptic thresholds no learning takes place. Thus, when the input is not present and the cortex is covered by the activity depression no learning will take place. Looking at the post-synaptic learning situation in figure 20 it is also clear that even as the activity levels recover to there noise levels the weights cannot begin to recover the other way until the post-synaptic activity is above the high post-synaptic threshold. Since this has been set above the noise level this will not happen until a new input stimulus is present. This means that when the activity level have recovered the weight values will still be at there respective minimal and maximal values and not the initial values.

If the respective minimal and maximal weight values were taken to be the initial weights then the connections' weights would end at these values after wave propagation. In that case the initial state would again be reached for both weight and activity values once full recovery from the activity depression had taken place. However, this initial state would be the state in which the weights had already fully compensated for the activity depression before the propagation of the waves that cause it.

Another option would be to start the weights at their opposite extreme values. This would be the minimum for Hebbian connection and maximum for Anti-Hebbian. This means that the cortex begins in an unfavorable state for wave propagation. It was shown though simulation that the first input only causes initial activity which dies when the input is no longer present when starting in the unfavorable weight state. However, as seen in the weight frames of figure 38, even the small activity causes enough of an activity depression to drive the weight to a more favorable state. This state was favorable enough allow the follow up input at 400 ms to produce a wave. After the propagation of this first wave the resulting activity depression was not significantly different then that left after the first waves above. Thus, the weight compensation after the first successful wave was consistent with that above and the follow-up waves propagated as though the initial weight condition was not unfavorable. From this it can be said that learning allows the cortex to overcome the unfavorable initial weight state.

Still the learning scheme used above has no way of returning to these values during the absence of high activity. This is mainly due to the fact that no learning takes place when both pre and post-synaptic activities are below the low thresholds. It is a small alteration to the GENESIS Hebbian synaptic channel code to remove this restriction. This would produce the learning situation depicted in figure 39. Here the learning that takes place above both high thresholds is mirrored below both low thresholds. Thus, when there is no input stimulus present and the cortex activity has been driven down so that both pre and post-synaptic activity levels for all cells are very low, the cortex will react as if they are both high and return to the initial unfavorable state.

This would require a slight modification to the pre and post-synaptic learning schemes presented above since the

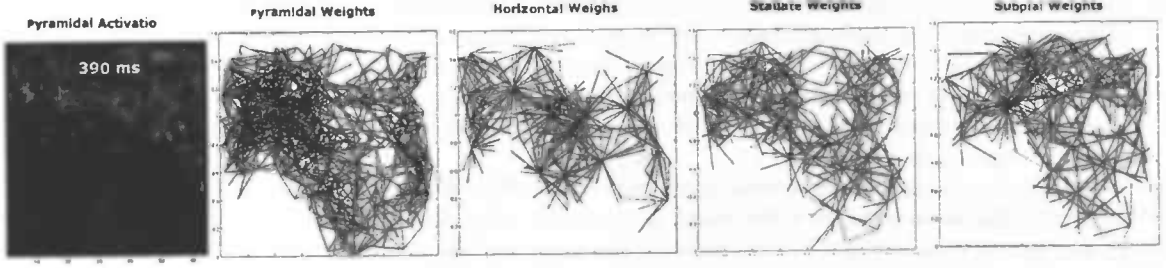

Figure 38: Frame showing the activity and weight state 240 ms after the end of the initial input pulse. The weights were initialized in an unfavorable state, with the pyramidal weights at their minimum values and the horizontal, stellate and subpial weights at there maximum values

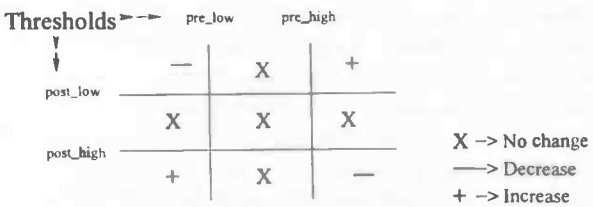

Figure 39: Diagram showing mirrored learning below both low thresholds

post and pre-synaptic activity thresholds are set respectively to unreachably low values. Hence, the weight values can never be below both the pre and post-synaptic values at the same time. However, it should be able to find reachable low values that are reached only when the weight recovery is desired.

4 Conclusion

The contributions of Hebbian learning to the model can best be viewed in terms of a comparison of the model response features before and after its implementation. Section 4.1 analyzes each result by making this comparison. The basic conclusion is that Hebbian learning has served to add to the understanding of the model characteristics. This motivates the continued inclusion of Hebbian learning in the model as the model an understanding of the turtle cortex evolve. Section 4.2 highlights the ways in which the model can evolve and the research presented in this paper can be expanded.

4.1 The Model Before and After Learning

Three main features of the model cortex have been discussed in this paper. First there exists a slight bias between the left and right LGN input locations. Secondly, an initial cortex activity wave is followed by an activity depression that suppresses further response to input stimulus. Most importantly in terms of encoding applications, the propagation characteristics of the cortex wave response encode the spatial location of its triggering LGN stimulus. Using these three cortex features as a basis the effects of Hebbian learning were analyzed. The results show that simple Hebbian learning can be used to compensate for undesirable characteristics while preserving even introducing new desirable ones.

To begin with, anti-Hebbian learning applied to the LGN-to-pyramidal connections that stimulate the cortex network was shown to serve as a mechanism for compensating for the input bias associated with the difference in

varicosities of left and right LGN cells in the input array. It can be argued that this bias reflects a known characteristic of the turtle cortex because it is a direct result of the known cortex axon distribution. Yet, it can also be argued this bias introduces an unwanted feature to the cortex model in terms of computational uses. Changing the varicosity distribution used in the model will reduce the accuracy of the model. However, it is not clear if the bias this introduces is a realistic feature of the model. Learning provides a way to eliminate the bias while sticking to the known structure of the cortex.

On the other hand, it is quite reasonable to view the fact that the activity depression following wave propagation prevents further wave response in the model as a negative feature of the model. Research on the real turtle cortex has not directly disproved this feature. In fact, activity depressions do follow activity waves in the real cortex. Yet total cortex numbing for a period as long as 2 seconds is hard to view as a realistic feature of the model. Even if this feature did reflect the behavior of the real cortex, it can be seen as undesirable in terms of encoding applications of the model. Thus, the anti-Hebbian/Hebbian learning scheme discussed above that removes this feature can be seen as an improvement to the model. Also, the idea that the competition between Hebbian and anti-Hebbian learning mechanisms is a key part of cortex behavior is becoming more accepted in cortex research.

The most interesting and, in terms of engineering applications, important feature of the cortex model is its ability to encode spatial information in the wave response. Thus it is quit important that this feature remain a part of the model. It was shown that synaptic learning changes some characteristics of the wave response in compensating for the activity depression but the characteristics most important in input distinction were preserved. The increased propagation speed of the waves may be seen biologically as reducing the time with which the information is present, and thus the ability to fully respond to the information. However, the increased differences between non-active and active cortex areas during learning wave propagation was shown to increase the information content throughout the wave propagation time. In the case of the left and right waves the time window in which the wave information was highest was shown to be equally to that of the non-learning waves. Thus, it can be argued that the wave information content has be compressed in time, but not decreased. Also, in terms of possible model applications, faster reaction time can be seen as an improvement as long as spatial distinction remains possible.

Finally, learning was able to introduce a biologically reasonable yet new feature to the model. A constant unchanging stimulus was shown to disrupt the learned activity depression compensation and prevent a second wave response without a sufficient break or location change in the input. Because of the localization of the wave response to the location of the cortex activity, once the information of the input has been encoded in an initial wave response, a change is needed to trigger further encoding. If the information does not change then the cortex does not continue to encode it. From both a biological and application perspective, responding to a change in input is more interesting then wasting cortical energy on recording an absence in change. Thus, not only does feature specific numbing bring the model a step closer to biology, it can be seen as improving the encoding mechanism. Cellular numbing is shown to be too global to be input location specific. The weight response numbing suggests a feasible feature specific numbing mechanism for wave response cortex networks.

The results of this paper cannot be said to provide a complete understanding of the role of Hebbian learning the turtle cortex model. Further understanding of the real turtle cortex is needed to validate the use of Hebbian learning in this model as an aid in understanding cortex behavior. Also, further exploration into the practical modeling issues, such as the briefly discussed issue of return to the initial weight state, needs to be done. However, while the full benefits and biological implications of introducing Hebbian learning mechanisms into the cortex model may still be unclear, the results presented in this paper motivate the possible gains to be made by the exclusion of such learning mechanisms in further models of this type.

4.2 Future Research Directions

Based on the results presented in this paper several future research directions can be suggested.

The results highlight the need for a better understanding of the synaptic properties of the real cortex. However, this could prove to be a difficult task. Recording short-term input responsive changes in synaptic properties would seem to be more difficult then recording the pyramidal cell activities. The results presented here and possible future results can aid in focusing the learning detection methods. For instance, the results suggest that the synaptic properties may be different before and after the propagation of an activity wave.

Only several Hebbian learning variations designed to accomplish specific tasks have been explored so far with the cortex model. Further variation of the learning parameters and the introductions of new learning schemes will undoubtedly reveal further limitations and possibilities of learning in manipulating the model features.

Also, exploration of possible applications for such a wave-encoding model will help define desired model features beyond the features of the real cortex. Based on the new goals, learning schemes that go beyond the limits of Hebbian learning can be explored.

By adding a retina model to initially encode visual scenes before the information is passed on through the LGN cells to the cortex the biological significance of the model can be further explored while expanding the application possibilities. Eventually, a model of the full visual pathway that can encode complex visual scenes and decode relevant information from them is desired.

The results presented in this paper suggest that continuing to include learning in the model as it evolves will help to illuminate its features and limitations.

References

[1] James M. Bower, David Beeman, "The Book of GENESIS", Second Edition, *TELOS, NewYork* (1998).

[2] Gal Chechik, Isaac, Meilijson, "Synaptic Pruning in Development: A Novel Account in Neural Terms", *Neural Computation, 10(7), 1759-1777*, (1998).

[3] K. X. Du, B. K. Ghosh, "Decoding the position of a Visual Stimulus from Cortical Waves of Turtles", *Computational Neuroscience Meeting* (2002).

[4] K. X. Du, B. K. Ghosh, P. S. Ulinski, "Encoding and Decoding Target Locations Waves in the Turtle Visual Cortex", *accepted by IEEE Transactions on Biomedical Engineering* (2004).

[5] K. X. Du, B. K. Ghosh, P. S. Ulinski, "Motion Encoding and Decoding with Spatiotemporal Waves in the Turtle Visual Cortex", *Submitted to IEEE Transactions on Biomedical Engineering* (2004).

[6] F. Galan, M. Weidert, R. Menzel, A. Herz, G. Galizia, "Hebbain Reverberations in an Insects Brain".

[7] A. Gopnic, A. Meltzoff, P. Kuhl, "The Scientist in the Crib: What Early Learning Tells Us About the Mind", *New York, NY: HarperCollins Publishers* (1999).

[8] Simon Haykin, "Neural Networks: A Comprehensive Foundation", Second Edition, 1999.

[9] Erin Hoiland, "Brain Plasticity: What is it?", *http://faculty.washington.edu/chudler/plast.html#fact. prepared by Erin Hoiland.*

[10] D. Hubel, "Eye, Brain and Vision", *Scientific American Library* (1995).

[11] M. Kac, "Can One Hear Shape of a Drum", *AMERICAN MATHEMATICAL MONTHLY 73* (1966).

[12] Eric R. Kandel, James H. Schwarts, Thomas M. Jessell, "Principles of Neural Science", Second Edition, (1991).

[13] Eric R. Kandel, Brain and Behavior*In: Eric R. Kandel, James H. Schwarts, Thomas M. Jessell, eds. "Principles of Neural Science", Second Edition, 1991.*

[14] Eric R. Kandel, Steven A. Siegelbaum, James H. Schwarts, Synaptic Transmission, *In: Eric R. Kandel, James H. Schwarts, Thomas M. Jessell, eds. "Principles of Neural Science", Second Edition, 1991.*

[15] Eric R. Kandel, Thomas Jessell, Early Experience and the Fine tuning of Synaptic Connections, *In: Eric R. Kandel, James H. Schwarts, Thomas M. Jessell, eds. "Principles of Neural Science", Second Edition, 1991.*

[16] Wolfgang Maass, Christopher M. Bishop, "Pulsed Neural Neworks", MIT Press, (1999).

[17] P. S. Mazurskaya, "Birth of a Learning Law", *Neurosci. Behav. Physiol. 7, p311-318* (1974).

[18] David A. Medler, "What are Artificial Neural Networks?", www.neuron-ai.tuke.sk, section 2.2.3.2.

[19] K. F. Moran, M. A. Andrade, "Receptive Field Map Development by Anti-Hebbian Learning", *Elsevier Science Aug;10(6):1037-1052* (1997).

[20] K. A. Mulligan, P. S. Ulinski, "Organization of geniculocortical projections in turtles: isoazimuth lamellae in the visual cortex", *J. Comp. Neurol.* 269 (1990) 531-547.

[21] Z. Nenadic, Bijoy K. Ghosh, Philip S. Ulinski, "Modeling and Estimation Problems in the Turtle Cortex", *IEEE Tran. Bio-Med Eng. Vol. 49. No. 8*, August 2002. pp 753-762.

[22] Z. Nenadic, Bijoy K. Ghosh, Philip S. Ulinski, "Propagation Waves in Visual Cortex: A Large Scale Turtle Visual Cortex", *J. of Computational Neuroscience*, Vol. 14, pp.161-184,2003.

[23] J. C. Prechtl, L. B. Cohen, P. P. Mitra, B. Pesaran, D. Kleinfeld, "Visual Stimuli Induce Waves of Electrical Activity in turtle visual cortex", *Proc. Natl. Acad. Sci. U.S.A. Vol.94, pp.7621-7626* (1997).

[24] K. A. Robbins, "Visualization of Scientific Video Data Using KL Decomposition" ,*IEEE Transactions on Visualization and Computer Graphics, volume 4, Issue 4, PP. 330-343, ISSN:1077-2626* (1998).

[25] K. S. Grossberg, "Birth of a Learning Law", *Technical Report CAS/CNS-TR-97-017* (1997).

[26] D. M. Senseman, "Correspondence between visually envoked voltage sensitive dye signals and synaptic activity recorded in cortical pyramidal cells with intracellular microelectrodes", *Vis. Neurosci., 13* (1996) 963-977.

[27] D. M. Senseman, "Spatiotemporal structure of depolarization spread in cortical pyramidal cell populations evoked by diffuse retinal flashes",*Vis. Neurosci., 16* (1999) 65-79.

[28] D. M. Senseman, K. A. Robbins, "Modal Behavior of Cortical Neural Networks during Visual Processing " ,*J. of Neurosci., 19:RC3:1-7* (1999).

[29] G. Tortora, S. Grabowski, "Principles of Anatomy and Physiology",(8th ed.), *New York: HarperCollins College Publishers* (1996).

[30] P. S. Ulinski, "The cerebral Cortex in Reptiles", *In: Jones E G, Peters A, eds. Cerebral Cortex. Vol 8A* (1990).

[31] P. S. Ulinski, "Neural Mechanisms Underlying the analysis of Moving Visual Stimuli", *In: Ulinski S, Jones E G, Peters A, eds. Cerebral Cortex. Vol 13* (1999).

[32] Wenxue Wang, Bijoy K. Ghosh, Philip S. Ulinski, "Cellular Mechanisms Cotrolling Propagation in Visual Cortex", *Submitted to Journal of Computational Neuroscience.*

[33] http://www.all-science-fir-projects.com, "Connectionism".

[34] http://www.all-science-fir-projects.com, "Hebbian Learning".

[35] http://www.colinfahey.com/../ 2003apr20_neuron.htm

[36] http://faculty.washington. edu/chudler, "Brain Facts and Figures ", *maintained by Eric H. Chudler, PhD.* .

[37] http://happyturtle.ms11.net, "Turtle Anatomy", *Online Information Site: www.web.ms11.net/happyturtle.*

[38] http://hypertextbook.com, "The Pysics Factbook / Mass of a Human Brain ", *Edited by Glenn Elert – Written by his students* .

[39] http://ncca.bournemouth.ac.uk/.../ major.dir/annet.html

[40] http://www.permutationcity.co.uk/projects/neural, Permutation City, "Organization of Receptive Fields in the Forebrain of Emys Orbiculari", *copywrite Matthew Caryl.*

[41] "A Brief History of Connectionism", www.psychology.mcmaster.ca.sk.

[42] http://serendip.brynmawr.edu/bb, "Brain and Behavior", *Serendip.*

[43] http://serendip.brynmawr.edu/bb/kinser/images/braingroup7.jpg

[44] http://www.wcsscience.com/brain, "The Brain", *content by Bill Willis* (2002).

[45] http://www.wcsscience.com/brain/page.html

[46] http://www.willamette.edu/ gorr/classes/cs449/motivate.htm